

# 1 **The macronutrient and micronutrient (iron and manganese) content** 2 **of icebergs**

3 Jana Krause<sup>1</sup>, Dustin Carroll<sup>2</sup>, Juan Höfer<sup>3,4</sup>, Jeremy Donaire<sup>5,6</sup>, Eric P. Achterberg<sup>1</sup>, Emilio Alarcón<sup>4</sup>, Te  
4 Liu<sup>1</sup>, Lorenz Meire<sup>7,8</sup>, Kechen Zhu<sup>9</sup>, Mark J. Hopwood<sup>9\*</sup>

5 <sup>1</sup>GEOMAR Helmholtz Centre for Ocean Research Kiel, Kiel, Germany

6 <sup>2</sup>Moss Landing Marine Laboratories, San José State University, Moss Landing, California, USA

7 <sup>3</sup>Escuela de Ciencias del Mar, Pontificia Universidad Católica de Valparaíso, Valparaíso, Chile

8 <sup>4</sup>Centro FONDAP de Investigación en Dinámica de Ecosistemas Marinos de Altas Latitudes (IDEAL), Valdivia, Chile

9 <sup>5</sup>Facultad de Ingeniería, Universidad Andrés Bello, Viña del Mar, Chile

10 <sup>6</sup>Faculty of Sciences and Bioengineering Sciences, Vrije Universiteit Brussel, Brussels, Belgium

11 <sup>7</sup>Department of Estuarine and Delta Systems, Royal Netherlands Institute for Sea Research, Yerseke, The Netherlands

12 <sup>8</sup>Greenland Climate Research Centre, Greenland Institute of Natural Resources, Nuuk, Greenland

13 <sup>9</sup>Department of Ocean Science and Engineering, Southern University of Science and Technology, Shenzhen, China

14 *Correspondence to:* Mark J. Hopwood (Mark@sustech.edu.cn)

15 **Abstract.** Ice calved from the Antarctic and Greenland Ice Sheets or tidewater glaciers ultimately melts  
16 in the ocean contributing to sea-level rise and potentially affecting marine biogeochemistry. Icebergs have  
17 been described as ocean micronutrient fertilizing agents, and biological hotspots due to their potential  
18 roles as platforms for marine mammals and birds. Icebergs may be especially important fertilizing agents  
19 in the Southern Ocean, where availability of the micronutrients iron and manganese extensively limits  
20 marine primary production. Whilst icebergs have long been described as a source of iron to the ocean,  
21 their nutrient load is poorly constrained and it is unclear if there are regional differences. Here we show  
22 that 589 ice fragments collected from calved ice in contrasting regions spanning the Antarctic Peninsula,  
23 Greenland, and smaller tidewater systems in Svalbard, Patagonia and Iceland have similar (micro)nutrient  
24 concentrations with limited or no significant differences between regions. Icebergs are a minor or  
25 negligible source of macronutrients to the ocean with low concentrations of  $\text{NO}_x^-$  ( $\text{NO}_3^- + \text{NO}_2^-$ , median  
26  $0.51 \mu\text{M}$ ),  $\text{PO}_4^{3-}$  (median  $0.04 \mu\text{M}$ ), and dissolved Si (dSi, median  $0.02 \mu\text{M}$ ). In contrast, icebergs deliver  
27 elevated concentrations of dissolved Fe (dFe, median  $12 \text{ nM}$ ) and Mn (dMn, median  $2.6 \text{ nM}$ ). Sediment  
28 load for Antarctic ice (median  $9 \text{ mg L}^{-1}$ ,  $n=144$ ) was low compared to prior reported values for the Arctic  
29 (up to  $200 \text{ g L}^{-1}$ ). Whilst total dissolvable Fe and Mn retained a strong relationship with sediment load

30 (both  $R^2 = 0.43$ ,  $p < 0.001$ ), weaker relationships were observed for dFe ( $R^2 = 0.30$ ,  $p < 0.001$ ), dMn ( $R^2 =$   
31  $0.20$ ,  $p < 0.001$ ) and dSi ( $R^2 = 0.29$ ,  $p < 0.001$ ). A tight correlation between total dissolvable Fe and Mn ( $R^2$   
32  $= 0.95$ ,  $p < 0.001$ ) and a total dissolvable Mn:Fe ratio of 0.024 suggested a lithogenic origin for the majority  
33 of sediment present in ice. Dissolved Mn was however present at higher dMn:dFe ratios, with meltwater  
34 fluxes roughly equivalent to 30% of the corresponding dFe flux. Our results demonstrated that the nutrient  
35 concentrations measured in calved icebergs are consistent with an atmospheric source of  $\text{NO}_x^-$  and  $\text{PO}_4^{3-}$   
36 . Conversely, high Fe and Mn, and occasionally high dSi concentrations, are associated with englacial  
37 sediment, which experiences limited biogeochemical processing prior to release into the ocean.

## 38 **1 Introduction**

39  
40 At the interface between the cryosphere and ocean, icebergs are both physical and chemical agents via  
41 which ice-ocean interactions affect marine biogeochemical cycles (Enderlin et al., 2016; Helly et al.,  
42 2011; Smith Jr. et al., 2007). Icebergs are often described as fertilizing agents, especially in the context  
43 of the Southern Ocean (Schwarz and Schodlok, 2009; Smith Jr. et al., 2007; Vernet et al., 2011).  
44 However, the fertilizing effect of icebergs is likely regionally dependent due to changes in the identity of  
45 the (micro)nutrients limiting marine primary production, and perhaps also due to regional changes in the  
46 nutrient load of icebergs. In the Southern Ocean, iron (Fe) is thought to be the main nutrient limiting  
47 phytoplankton growth throughout much of the growth season and so changes to regional Fe supply can  
48 have ecosystem effects (Martin et al., 1990a, b; Moore et al., 2013). A critical research challenge is  
49 therefore to constrain Fe sources and sinks in the Southern Ocean and to assess their climatic sensitivity  
50 (Martin, 1990; Wadley et al., 2014). Icebergs are one such Fe source to pelagic ecosystems (Raiswell,  
51 2011; Raiswell et al., 2008; Shaw et al., 2011). Icebergs have long been described as an important Fe  
52 source via delivery of both englacial sediment and the dissolved components of ice melt (Hart, 1934; Lin  
53 et al., 2011; Raiswell et al., 2008). Positive chlorophyll anomalies following iceberg passage in the  
54 Southern Ocean during the growth season have been detected by satellite-derived chlorophyll  
55 measurements and these are usually attributed to Fe-fertilization (Schwarz and Schodlok, 2009; Wu and  
56 Hou, 2017). However, Fe may not be the only micronutrient to limit marine primary production around

57 Antarctica. Recent work has suggested that low dissolved manganese (Mn) concentrations are a further  
58 co-limiting factor for phytoplankton growth in parts of the Southern Ocean (Browning et al., 2021; Hawco  
59 et al., 2022; Latour et al., 2021). As Fe and Mn share similar sources, icebergs might also be an equally  
60 important source term for the polar marine Mn cycle (Forsch et al., 2021).

61  
62 In contrast to Antarctica, Fe-limitation of marine phytoplankton growth in the Arctic is a less prominent  
63 feature. Fe-limitation is sparsely reported in the Arctic (Taylor et al., 2013) and largely confined to  
64 offshore areas of the high-latitude North Atlantic away from typical iceberg trajectories (Nielsdottir et al.,  
65 2009; Ryan-Keogh et al., 2013). Phytoplankton growth within regions around Greenland affected by  
66 icebergs is more often limited by nitrate availability (Randelhoff et al., 2020, Krisch et al., 2020). With  
67 icebergs thought to supply only limited concentrations of nitrate and phosphate to the ocean, a direct  
68 iceberg fertilization effect is not expected in nitrate-limited marine regions (Shulenberger, 1983). The  
69 macronutrient content of icebergs is however poorly constrained, especially for components other than  
70 Fe. Although subject to large uncertainties, icebergs could be a modest source of silica to the marine  
71 environment (Hawkings et al., 2017; Meire et al., 2016) which might have ecological effects. Whilst high  
72 macronutrient concentrations are found throughout the Southern Ocean, dissolved silica (dSi) availability  
73 often limits diatom growth in the Arctic due to its depletion prior to nitrate (Krause et al., 2018, 2019).

74  
75 In order to understand how iceberg-derived fluxes of (micro)nutrients may change regionally with climate  
76 change and glacier retreat inland, it is necessary to understand the origin and fate of nutrients within  
77 calved icebergs at sea. The ultimate origin of nutrients in icebergs could be argued to be atmospheric  
78 (Fischer et al., 2015; Hansson, 1994). Inland precipitation and aerosol deposition on ice surfaces will  
79 exert a large influence on the nutrient content of bulk ice which is ultimately calved into the ocean as  
80 icebergs (Vernet et al., 2011). However, processes beyond the ice-atmosphere interface may also affect  
81 the nutrient content of ice. Furthermore, internal cycling may also critically redistribute (micro)nutrients  
82 and affect the relative abundance of elements in both dissolved ( $<0.2 \mu\text{m}$ ) and particulate ( $>0.2 \mu\text{m}$ )  
83 phases. Landslides onto ice surfaces, and the movement of basal ice over bedrock or subglacial sediments  
84 create layers of ice visibly enriched in sediment (Alley et al., 1997; Knight, 1997; Mugford and

85 Dowdeswell, 2010). Some fraction of the labile phases in these sediments; particularly for the elements  
86 Fe, Mn and silica, which are present at high abundances; may ultimately be transformed into bioaccessible  
87 nutrients in the ocean (Forsch et al., 2021; Hawkings et al., 2017; Raiswell, 2011). How sediment is  
88 gained and lost from ice before, during and after iceberg calving therefore might exert some influence on  
89 measured (micro)nutrient concentrations in melting icebergs at sea (Hopwood et al., 2019).

90

91 On exposed ice surfaces during the growth season, cryoconite formation and the growth of algae are  
92 notable features which will act to re-distribute nutrients between inorganic and organic pools and to  
93 amplify heterogeneity in the distribution of nutrients within ice (Cook et al., 2015; Rozwalak et al., 2022;  
94 Stibal et al., 2017). These processes will occur alongside, and likely interact with, other photochemical  
95 reactions (Kim et al., 2010; Kim et al., 2024). Whilst iceberg calving may temporarily disturb features  
96 present on ice surfaces, and the rolling of smaller icebergs will regularly interrupt cryoconite growth on  
97 calved ice surfaces, long-lived icebergs may continue to accumulate the effects of photochemical  
98 processes and re-develop cryoconite. The nutrient content of icebergs, nutrient distributions and their  
99 ratios might therefore not be static and in fact subject to semi-continuous changes. As ice moves  
100 downstream from ice sheets to the coastline, critical physical processes may exert a strong influence on  
101 the characteristics of the ice which ultimately calves into the ocean (Smith et al., 2019). At the base of  
102 floating ice tongues and ice shelves, the melt-rates of basal ice layers exposed to warm ocean waters can  
103 be rapid. Beneath the floating ice tongue of Nioghalvfjærdsbræ in northeast Greenland, for example, a  
104 melt rate of  $8.6 \pm 1.4$  m year<sup>-1</sup> is likely sufficient to remove most sediment-rich basal ice prior to iceberg  
105 calving (Huhn et al., 2021). In other similar cases worldwide, calved ice may ultimately be deprived of  
106 basal layers which might otherwise have carried distinct labile sediment loadings reflecting subglacial  
107 processes (Smith et al., 2019). Nevertheless, post-calving the nutrient content of ice may still be strongly  
108 affected by ‘new’ ice-sediment interactions. Icebergs which become grounded, or scour shallow coastal  
109 sediments, may temporarily re-acquire a basal layer loaded with sediment (Gutt et al., 1996; Syvitski et  
110 al., 1987; Woodworth-Lynas et al., 1991). Scoured sediments may be physically and chemically distinct  
111 from those acquired from land-slides or basal glacial processes and thus also temporarily introduce  
112 different nutrient ratios and concentrations in ice and melt water (Forsch et al., 2021). Finally, whilst

113 many research questions concerning the effects of the cryosphere on the ocean relate to melting processes,  
114 marine ice formation is a mechanism via which ice growth can occur in the water column (Craven et al.,  
115 2009; Lewis and Perkin, 1986; Oerter et al., 1992). Marine ice is formed from supercooled seawater  
116 around Antarctica via the formation of platelet, or frazil, ice crystals. Whilst the chemical composition of  
117 this ice is poorly studied, measurements from the Amery Ice Shelf suggest marine ice has relatively high  
118 dissolved Fe (dFe) concentrations (e.g. 339-691 nM dFe, Herraiz-Borreguero et al., 2016). The origin of  
119 this dFe may be subglacial, potentially indicating a synergistic effect between subglacial and ice melt Fe  
120 sources. Similar synergistic effects have been suggested from model studies concerning sea ice and ice  
121 shelves, whereby sea ice may trap and later release Fe that originates from ice shelves (Person et al.,  
122 2021). A ‘source-to-sink’ narrative concerning iceberg-derived (micro)nutrient delivery from ice directly  
123 into the ocean may therefore be over-simplistic. It is important to recognise that the extent of spatial and  
124 temporal overlap between different (micro)nutrient sources may result in interactive effects in annual  
125 budgets. Such effects could arise due to the underlying physical processes and/or the seasonal timing of  
126 micro(nutrient) sources and sinks (Boyd et al., 2012; Person et al., 2021).

127

128 The (micro)nutrient content of icebergs and the associated fluxes of (micro)nutrients to the marine  
129 environment have been commented on around Greenland, Antarctica, and in smaller catchments around  
130 Svalbard (Cantoni et al., 2020; Nomura et al., 2023; Smith Jr. et al., 2007). Icebergs are widely thought  
131 to constitute a major source of Fe, particularly particulate Fe, to the ocean (Lin et al., 2011; Lin and  
132 Twining, 2012; Raiswell et al., 2016). We hypothesize that dMn, which shares similar sources with dFe,  
133 but is less susceptible to scavenging in the ocean, may also be delivered by icebergs with comparable  
134 annual fluxes to dFe. Several studies have also hinted at considerable dSi (up to 10  $\mu$ M, Meire et al.,  
135 2016) or bioaccessible nitrogen concentrations (up to 5  $\mu$ M) within ice (Parker et al., 1978; Vernet et al.,  
136 2011). Macronutrient concentrations in glacial ice are primarily hypothesized to reflect atmospheric  
137 deposition (Vernet et al., 2011), but it is unclear whether or not concentrations in calved ice largely reflect  
138 those originally deposited on ice sheet surfaces. The extent to which sediment incorporation into ice  
139 affects nutrient dynamics in ice melt also remains unclear. Are macronutrient and micronutrient  
140 concentrations in ice comparable at regional scales, or are there important regional differences due to

141 changes in basal ice layer thickness, sediment load, and sediment acquisition/loss processes in nearshore  
142 waters between regions? Calved ice from small marine-terminating glaciers in Svalbard, for example, can  
143 have extremely high sediment loads of up to 200 g L<sup>-1</sup> (Dowdeswell and Dowdeswell, 1989), compared  
144 to lower values of 0.6-1.2 g L<sup>-1</sup> in the Weddell Sea (Shaw et al., 2011). Are higher sediment loads also  
145 accompanied by increased concentrations of dissolved silica and trace metals in ice melt? Or,  
146 alternatively, is the loss of sediment from ice too fast, and any associated chemical weathering processes  
147 too slow, to significantly affect the composition of ice melt?

148

149 In order to evaluate whether or not there are regional differences in the (micro)nutrient content of icebergs  
150 and the associated fluxes into the ocean, here we assess the concentration of macronutrients (NO<sub>x</sub><sup>-</sup>, dSi  
151 and PO<sub>4</sub><sup>3-</sup>), micronutrients (dissolved Fe and Mn) and total dissolvable metals (Fe and Mn) from calved  
152 ice across multiple Arctic and Antarctic catchments. In order to investigate potential spatial and temporal  
153 biases associated with seasonal shifts and the general targeting of smaller ice fragments to collect samples,  
154 we include repeat samples from five campaigns in Nuup Kangerlua (a fjord hosting three marine-  
155 terminating glaciers in southwest Greenland) and a comparison of recently calved ice from inshore and  
156 offshore ice samples in Disko Bay (west Greenland). Throughout, we test the null hypothesis that icebergs  
157 from different regions have no differences in macronutrient or micronutrient (Fe and Mn) concentrations.

## 158 **2 Methods**

### 159 **2.1 Sample collection**

160 Iceberg samples were collected by hand or by using nylon nets to snag ice floating fragments. Sample  
161 collection was randomized at each field site location (Fig. 1 and Supp. Table 1) by collecting ice samples  
162 at regular intervals along pre-defined transects. 1–5 kg ice pieces were retained in low-density  
163 polyethylene (LDPE) bags and melted at room temperature. The first 3 aliquots of meltwater were  
164 discarded to rinse the LDPE bags. Meltwater was then syringe filtered (0.2 μm, polyvinyl difluoride,  
165 Millipore) into pre-cleaned 125 mL LDPE bottles for dissolved trace metal analysis and 20 mL  
166 polypropylene tubes for dissolved nutrient analysis. All plasticware for trace metal sample collection was

167 pre-cleaned using a three-stage protocol: detergent, 1 week soak in HCl (1 M reagent grade), and 1 week  
168 soak in HNO<sub>3</sub> (1 M reagent grade) with three deionized water rinses after each stage. Filters for trace  
169 metal analysis were pre-rinsed with HCl (1 M reagent grade) followed by deionized water. Some  
170 unfiltered samples were also retained for total dissolvable metal analysis.

171  
172 In Disko Bay (west Greenland), a targeted exercise was conducted to test whether distinct regional  
173 patterns of ice nutrient concentrations could be associated with specific calving locations. During cruise  
174 GLICE (R/V Sanna, August 2022) ice collection was conducted as per other regions close to the outflow  
175 of Sermeq Kujalleq (also known as Jakobshavn Isbræ) and Eqip Sermia (Supp. Table 1). Additionally,  
176 ice fragments were collected from two large icebergs in Disko Bay, referred to herein as fragments from  
177 Iceberg "Beluga" and Iceberg "Narwhal". These icebergs were tracked using the ship's radar by logging  
178 the coordinates and relative bearing of the approximate centre of the iceberg at regular time intervals. In  
179 Nuup Kangerlua (southwest Greenland), samples were collected on 5 repeated campaigns spanning boreal  
180 spring and summer in different years (May 2014, July 2015, August 2018, May 2019 and September  
181 2019) to assess the reproducibility of data from the same region by different teams deploying the same  
182 methods in different months and years.

183

## 184 **2.2 Sediment load measurements**

185 Wet sediment sub-samples were dried at 60°C to determine sediment load (dry weight of sediment per  
186 unit volume, mg L<sup>-1</sup>). Sediment load was determined for a subset of randomly collected ice samples in  
187 parallel with (micro)nutrients in the Antarctic Peninsula. In Maxwell Bay (King George Island), a targeted  
188 exercise was conducted to collect ice with embedded sediment. Eight large ice fragments (10-45 kg) with  
189 sediment layers embedded within the ice were retained in sealed opaque plastic boxes. These fragments  
190 were specifically selected to avoid the possibility of including samples with surface sediment acquired by  
191 ice scouring the coastline or shallow sediments. Boxes were half-filled with seawater from the bay.  
192 Sediment-rich ice was left to melt in the dark with an air temperature of ~5-10°C. Periodically (after 2, 4,  
193 8, 16, 24, and 48 hours) the water was weighed and settled sediment was removed by decanting and  
194 filtration before estimating its dry weight.

### 196 **2.3 Chemical measurements**

197 Dissolved trace metal samples were acidified after filtration to pH 1.9 by addition of 180  $\mu$ L HCl (UPA,  
198 ROMIL) and allowed to stand upright for >6 months prior to analysis. Unfiltered trace metal samples  
199 were acidified similarly and trace metals in these samples are subsequently referred to as ‘total  
200 dissolvable’; defined as dissolved metals plus any additional metals present which are soluble at pH 1.9  
201 after 6 months of storage. Analysis via inductively-coupled, plasma mass spectrometry (ICP-MS, Element  
202 XR, ThermoFisher Scientific) was undertaken after dilution with indium-spiked 1 M HNO<sub>3</sub> (distilled in-  
203 house from SPA grade HNO<sub>3</sub>, Roth). 4 mL aliquots of total dissolvable samples were filtered (0.2  $\mu$ m,  
204 polyvinyl difluoride, Millipore) immediately prior to analysis.

205

206 Calibration for Fe and Mn was via standard addition with a linear peak response from 1–1000 nM ( $R^2 >$   
207 0.99). Analysis of the reference material CASS-6 yielded a Fe concentration of  $26.6 \pm 1.2$  nM (certified  
208  $27.9 \pm 2.1$  nM) and a Mn concentration of  $37.1 \pm 0.83$  nM (certified  $40.4 \pm 2.18$  nM). Due to the very  
209 broad range of Fe concentrations in ice samples, samples were run using varying dilution factors.  
210 Precision is improved at low dilution factors so we report results from the lowest dilution factor that could  
211 be used to keep Fe and Mn concentrations within the calibrated range (in many cases dissolved samples  
212 could be run without dilution). Dissolved samples were initially run at a tenfold dilution, using 1 M HNO<sub>3</sub>.  
213 A 1 M HNO<sub>3</sub> blank from the same acid batch was analysed every 10 samples and in triplicate at the start  
214 and end of each sample rack (90  $\times$  4 mL sample vials). Total dissolvable samples (unfiltered, acidified  
215 samples) were initially run at a hundredfold dilution followed by a tenfold dilution for samples with  
216 nanomolar concentrations. Samples with measured concentrations of Fe or Mn <25 nM were then re-run  
217 without dilution. Detection limits, assessed as 3 standard deviations of blank (1 M HNO<sub>3</sub>) measurements,  
218 varied between batches (and dilution factors) but were invariably <0.86 nM dFe and <0.83 nM dMn for  
219 the standard tenfold dilution analyses. The field blank (deionized water filtered and processed as a sample)  
220 was below the detection limit. As in a majority of cases samples were run by dilution, the 1 M HNO<sub>3</sub> acid  
221 used to both dilute samples and run as a reagent blank every 10 samples was therefore considered the



222 most useful blank measurement. Mean ( $\pm$ standard deviation) blank (1 M HNO<sub>3</sub>) measurements varied by  
223 acid batch from  $0.06 \pm 0.02$  nM dFe,  $0.03 \pm 0.02$  nM dMn; to  $0.38 \pm 0.08$  nM dFe, and  $0.14 \pm 0.08$  nM  
224 dMn.

225  
226 Where macronutrient samples were not collected in parallel with trace metals, samples preserved for trace  
227 metals were analysed for PO<sub>4</sub><sup>3-</sup> and dSi (this was not possible for NO<sub>x</sub><sup>-</sup> because of residual contamination  
228 from concentrated HNO<sub>3</sub> in LDPE bottles). Analysis of macronutrients was conducted for NO<sub>3</sub><sup>-</sup>, NO<sub>2</sub><sup>-</sup>,  
229 PO<sub>4</sub><sup>3-</sup> and dSi by segmented flow injection analysis using a QUAATRO (Seal Analytical) auto-analyzer  
230 (Hansen and Koroleff, 1999). Recoveries of a certified reference solution (KANSO, Japan) were  $98 \pm 1\%$   
231 NO<sub>x</sub><sup>-</sup>,  $99 \pm 1\%$  PO<sub>4</sub><sup>3-</sup> and  $97 \pm 3\%$  dSi. Detection limits varied between sample batches and were  $<0.10$   
232  $\mu$ M NO<sub>x</sub><sup>-</sup>,  $<0.02$   $\mu$ M NO<sub>2</sub><sup>-</sup>,  $<0.10$   $\mu$ M PO<sub>4</sub><sup>3-</sup>, and  $<0.25$   $\mu$ M dSi.

233

## 234 **2.4 Data compilation**

235

236 In addition to new data from 367 new samples collected and analysed herein, existing comparable data  
237 was compiled from prior literature, most of which was processed in prior work by the same protocol in  
238 the same laboratories as herein (see Supp. Table 1). Inclusive of prior work, a total of 589 samples are  
239 available for interpretation (note that not all samples were analysed for all parameters so n varies between  
240 statistical analyses). Previously published data includes samples from Greenland, Svalbard, the Antarctic  
241 Peninsula, Patagonia and Iceland (De Baar et al., 1995; Campbell and Yeats, 1982; Forsch et al., 2021;  
242 Höfer et al., 2019; Hopwood et al., 2017, 2019; Lin et al., 2011; Loscher et al., 1997; Martin et al., 1990b).  
243 Altogether, 575 out of the 589 samples reported were collected and analysed as described herein at the  
244 same laboratories. Only 14 literature values were from other laboratories so there is a high degree of  
245 internal consistency in the methods used. Throughout concentrations are reported in units L<sup>-1</sup>, referring  
246 to the concentration measured in meltwater.

## 247 **2.5 Statistical analysis**

248

249 To test if icebergs had statistically significant regional differences in (micro)nutrient concentrations  
250 depending on their origin at a hemisphere, regional or catchment scale, a multivariate PERMANOVA  
251 was realized (function `adonis2` from `vegan` package, Oksanen et al., 2020) using the concentrations of  
252 trace metals (both dissolved and total dissolvable) and macronutrients ( $\text{NO}_x^-$ ,  $\text{PO}_4^{3-}$  and  $\text{dSi}$ ). Along with  
253 this analysis a non-metric MultiDimensional Scaling (nMDS, function `metaMDS` from `vegan` package,  
254 Oksanen et al., 2020) was used to compute the ordination of the iceberg samples depending on their  
255 nutrient concentrations. An nMDS is an unconstrained ordination analysis that assess the  
256 similarities/dissimilarities among datapoints only using the set of variables informing the ordination  
257 (herein macro- and micronutrients concentrations). The variables considered for the analysis are  
258 summarized in orthogonal dimensions showing the more similar datapoints as closer (groupings of  
259 datapoints with similar characteristics) within the space created by the orthogonal dimensions. The same  
260 analyses were used to assess differences in Disko Bay samples collected in August 2022, in this case  
261 comparing iceberg samples collected in inshore and offshore zones. In both cases subsequent ANOVA  
262 (aov function package `stats`) and a Tuckey test (`TukeyHSD` function package `stats`) were undertaken to  
263 test for significant differences in specific (micro)nutrient concentrations.

264  
265 The relationship between iceberg sediment load and the concentration of trace metals (both dissolved and  
266 total dissolvable) and macronutrients was determined by means of a linear regression (`lm` function  
267 package `stats`). For this analysis two outliers were removed from the dataset because their sediment load  
268 values were over an order of magnitude larger ( $50726 \text{ mg L}^{-1}$  and  $6128 \text{ mg L}^{-1}$ ) than other values (total  
269  $n=144$ ); including these two data points would have disproportionately skewed the relationships. Finally,  
270 to analyse how melting and sediment release rates changed over time using the incubations in Maxwell  
271 Bay, we used the same procedure as Höfer et al., (2018). In short, we first tested if the relationship between  
272 melting and sediment release rates and time better fitted a linear or exponential relationship using a  
273 second-order logistic regression. Then, we tested the fit of the selected relationship (exponential in this  
274 case) to see if the relationship was significant and determined the percentage of variance explained (`lm`  
275 function package `stats`). Since the initial conditions of each incubation (i.e. iceberg size, shape and initial  
276 sediment load) varied, the rates for each individual experiment were normalized by dividing each rate by

277 the maximum rate registered in the same incubation. All statistical analyses and figures (package ggplot2)  
278 were realized using R version 4.3.2 (R Core Team, 2023).

## 279 **3 Results**

### 280 **3.1 Nutrient distributions in the global iceberg dataset**

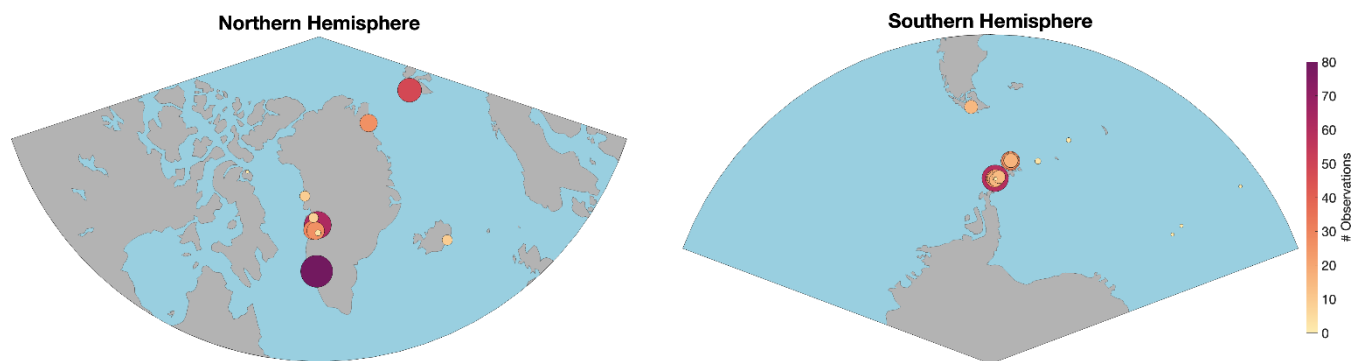
281 A total of 589 ice fragments have been analysed to date. The combined data is more balanced compared  
282 to prior work in terms of coverage of Antarctica (45% of samples), Greenland (42% of samples), Svalbard  
283 (8.1% of samples), and smaller sub-polar catchments in Patagonia, Canada, and Iceland (4.2% of  
284 samples). There are however still some spatial biases in the data. Notably samples from Greenland are  
285 largely from the west (Fig. 1), and samples from Antarctica are all from the Antarctic Peninsula or  
286 downstream waters along the “Iceberg Alley” in the Weddell Sea and the South Atlantic sector of the  
287 Southern Ocean (Tournadre et al., 2016). Almost all samples were collected in summer, with only a subset  
288 of samples (from Nuup Kangerlua, Supp. Table 4) collected in spring and autumn to investigate potential  
289 seasonal changes. At the catchment scale, Nuup Kangerlua (southwest Greenland, also known as  
290 Godthåbsfjord, 15% of the dataset), Eqip Sermia (west Greenland, 11% of the dataset), Thunder Bay  
291 (Western Antarctic Peninsula, 10% of the dataset), Kongsfjorden (Svalbard, 8.2% of the dataset), Disko  
292 Bay (west Greenland, 5.1% of the dataset), and Nelson Island (Northern Antarctic Peninsula, 5.1% of the  
293 dataset) are particularly well represented. The other 23 catchments each account for <5% of the samples.

294

295

296

297



298  
299

300 Figure 1. Sample distributions in the Northern and Southern Hemispheres. Literature values from prior  
301 work are included (see Supp. Table 1 for a full list of details).

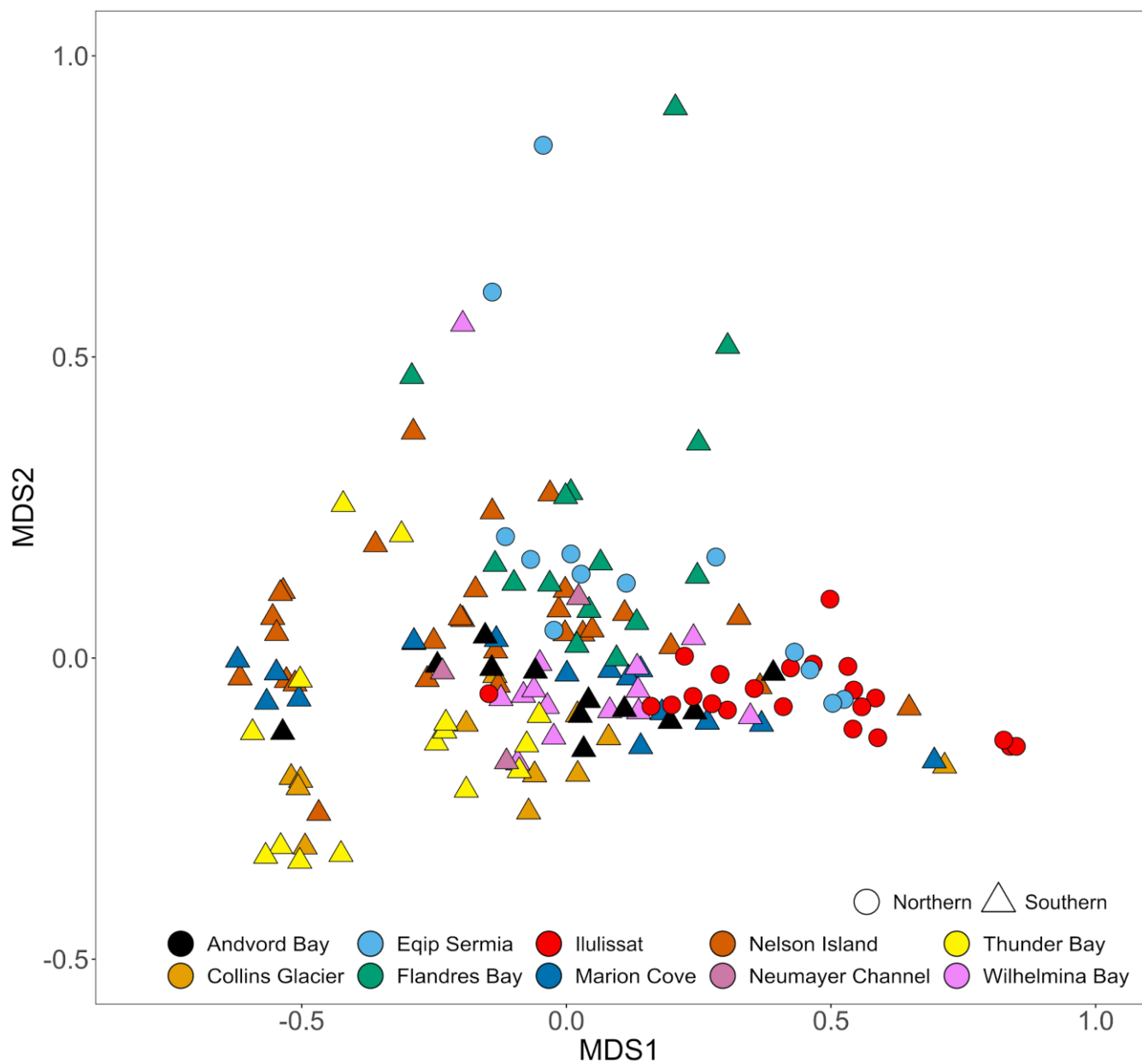
302

303 Average macronutrient concentrations in ice samples were low with median concentrations of  $0.04 \mu\text{M}$   
304  $\text{PO}_4^{3-}$ ,  $0.54 \mu\text{M}$   $\text{NO}_3^-$  and  $0.02 \mu\text{M}$  dSi. Throughout the dataset  $\text{NO}_2^-$  was close to, or below, detection  
305 thus  $\text{NO}_3^-$  and  $\text{NO}_x^-$  concentrations were practically identical with  $\text{NO}_2^-$  almost invariably constituting  
306  $<10\%$  of  $\text{NO}_x^-$  (mean 1.8%). Mean nutrient concentrations in all cases were higher than median  
307 concentrations and the large relative standard deviations indicated that variability between samples might  
308 mask any regional differences. Preliminary analysis revealed a large fraction of data below detection (i.e.  
309 concentrations  $<\text{LOD}$ ) for several components particularly  $\text{PO}_4^{3-}$  (24% of all measurements  $<\text{LOD}$ ) and  
310 dSi (48% if all measurements  $<\text{LOD}$ ). Other (micro)nutrients were less affected by detection limits, e.g.  
311 only 8% of  $\text{NO}_x$  concentrations were  $<\text{LOD}$ . In any dataset with a large fraction of data  $<\text{LOD}$ , how these  
312 values are treated makes some difference to calculated statistics so reported averages vary for  $\text{PO}_4^{3-}$  and  
313 dSi depending on how LOD values are treated. Removing values  $<\text{LOD}$  entirely would skew the statistical  
314 analyses. For example, the median values reported above increase from  $0.04$  to  $0.05 \mu\text{M}$   $\text{PO}_4^{3-}$ , and  $0.02$   
315 to  $0.19 \mu\text{M}$  dSi if values  $<\text{LOD}$  are excluded. For consistency throughout all statistical analyses, a value  
316 of '0' was therefore used to represent LOD data.

317

318 It has been previously reported that both TdFe and dFe concentrations are extremely variable within ice  
319 samples collected at the same location (Hopwood et al., 2017; Lin et al., 2011). This remained the case

320 with the expanded dataset herein with notable differences between the mean (82 nM dFe, 13  $\mu$ M TdFe)  
321 and median concentrations (12 nM dFe, 220 nM TdFe) on a global scale. An extremely broad range of  
322 concentrations was also observed for both dissolved Mn (mean 26 nM, median 2.6 nM) and total  
323 dissolvable Mn (TdMn; mean 150 nM, median 10 nM). As per Fe, this reflected the skewed distribution  
324 of the dataset towards a low number of samples with extremely high concentrations. The highest 2% of  
325 TdMn samples accounted for 79% of the cumulative TdMn measured. Similarly, the highest 2% of TdFe  
326 samples accounted for 77% of the cumulative TdFe measured. Accordingly, there were very high relative  
327 standard deviations for both mean dMn ( $26 \pm 160$  nM) and TdMn ( $150 \pm 1500$  nM) which, as per Fe,  
328 remained high when data was grouped by region or catchment. Considering all (micro)nutrients  
329 measured, there were no significant differences in the iceberg chemical composition at a hemispheric (p  
330 value = 0.16) or regional (p value = 0.16) level. However, a PERMANOVA analysis showed significant  
331 differences ( $R^2 = 0.24$ , p value  $<0.001$ ) at a catchment level. Similarly, an nMDS analysis (stress = 0.07)  
332 showed that samples from the same catchment tended to be grouped closer together (Fig. 2) and in general  
333 Antarctic samples were distributed on the left side, whereas Arctic samples were more abundant on the  
334 right side of the ordination analysis (Fig. 2).



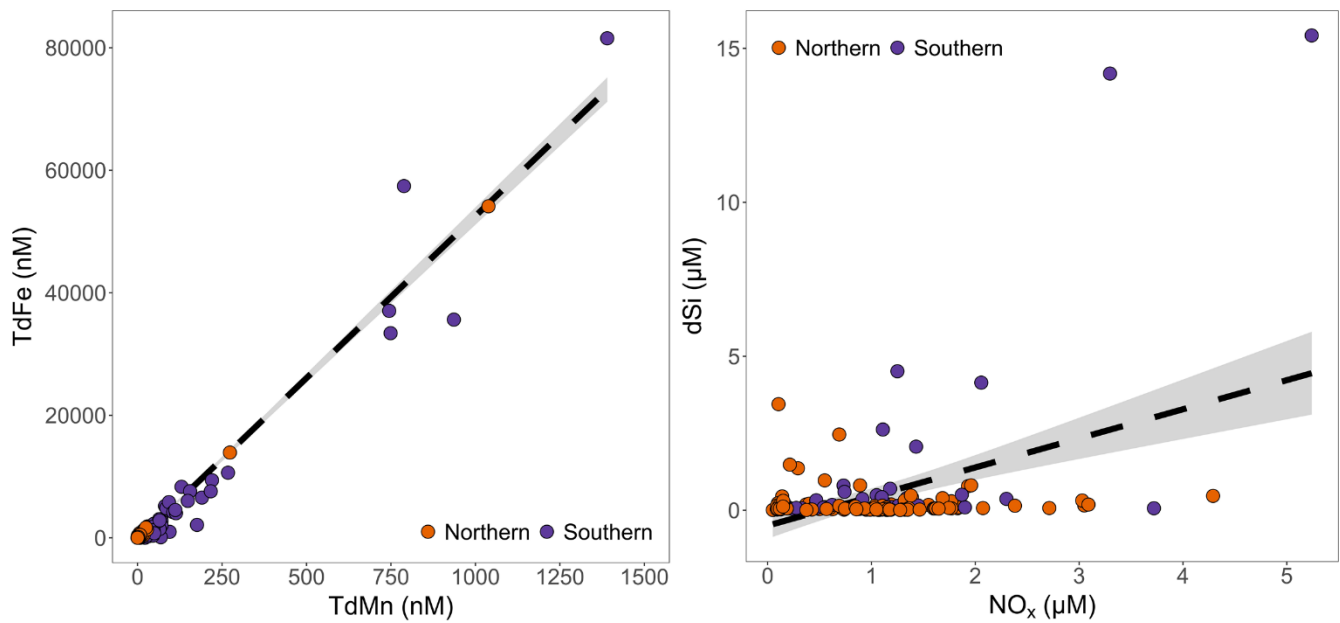
335

336 Figure 2. A scatter plot showing the results of an nMDS ordination analysis using macro- and  
 337 micronutrient concentrations. Only samples with complete data for the following parameters are shown:  
 338  $\text{NO}_x^-$ ,  $\text{PO}_4^{3-}$ , dSi, dFe, TdFe, dMn and TdMn. A non-metric MultiDimensional Scaling (nMDS) ordination  
 339 is used to represent multi-dimensional data in a reduced number of dimensions. MDS1 and MDS2 are  
 340 multidimensional scaling factors which represent the dissimilarities between the data sorted to catchment

341 level. Datapoints represent individual samples. Datapoints which appear further apart are more different,  
342 whereas those that cluster together are more similar. A PERMANOVA analysis of iceberg nutrient  
343 concentrations showed significant differences at a catchment level ( $R^2 = 0.24$ , p value  $<0.001$ ). Shapes  
344 denote hemispheres, while colours denote specific sampling locations.

345  
346 The ratio of TdFe:TdMn was linear ( $R^2 = 0.95$ , calculated excluding the highest 2% of Mn and Fe  
347 concentrations to avoid skewing the gradient, Fig. 3). Furthermore, the total dissolvable Mn:Fe ratio of  
348 0.0225 (linear regression  $\text{TdMn} = 0.0225 \times [\text{TdFe}]$ ) was close to mean continental crust composition  
349 which is approximately 0.1% MnO and 5.04% FeO by weight (producing a ratio of 0.020) (Rudnick and  
350 Gao, 2004). In contrast, no clear relationship was observed between dFe and dMn. For all data, all  
351 Antarctic data and all Greenlandic data, respectively, the mean dMn:dFe (0.47, 0.50 and 0.28) and median  
352 dMn:dFe (0.17, 0.19 and 0.11) ratios were however consistently higher than the TdMn:TdFe ratio. This  
353 indicates an excess of dMn compared to the lithogenic ratio observed in the total dissolvable fraction.

354  
355 Neither dMn or dFe correlated well with dSi. Throughout the whole dataset, dSi concentrations were low.  
356 Only 7 of 478 samples had dSi concentrations  $>10 \mu\text{M}$ , only 9.4% of samples had concentrations  $>1.0$   
357  $\mu\text{M}$ , and 48% of all samples were below detection. Dissolved Si therefore had concentrations and a  
358 distribution much more like  $\text{NO}_x^-$  and  $\text{PO}_4^{3-}$  than Mn or Fe. This was not typically the case in glacier  
359 runoff close to the sites where ice was collected (Supp. Table 2). With the exception of subglacial runoff  
360 collected on Doumer Island (South Bay, Western Antarctic Peninsula), dSi concentrations in runoff were  
361 always high relative to both nitrate in runoff (typically  $\sim 12 \times [\text{NO}_x^-]$ ) and to the mean dSi concentration  
362 in icebergs. Doumer Island consists of a small ice cap which is likely cold-based with steep topography,  
363 such that runoff-sediment interaction is likely limited.



364

365 Figure 3. A comparison of (micro)nutrient concentrations in all ice fragments where concentrations were  
 366 above the detection limits. *Left* Total dissolvable Fe and total dissolvable Mn were strongly correlated (p  
 367 value <0.001,  $R^2 = 0.95$ ), note the highest 2% of measured concentrations were excluded to avoid skewing  
 368 the gradient. *Right* dSi and  $\text{NO}_x^-$  had a weak correlation (p value <0.001,  $R^2 = 0.19$ ). The 95% confidence  
 369 interval is shaded in grey.

370

371 No significant relationship was evident between  $\text{PO}_4^{3-}$  and  $\text{NO}_x^-$  concentrations, whereas a weak, but  
 372 significant, relationship was evident between dSi and  $\text{NO}_x^-$  concentrations (Fig. 3). A subset of samples  
 373 appeared to show a close to 1:1 relationship between dSi and  $\text{NO}_x^-$ , which resembles the Redfield Ratio  
 374 (Redfield, 1934). A closer inspection of these points shows they accounted for about 14% of the sub-  
 375 dataset where all macronutrient concentrations were detectable (n=22 for those with  $[\text{NO}_x^-]$  and  $[\text{dSi}] > 0.4$   
 376  $\mu\text{M}$ , for lower concentrations it is largely arbitrary determining whether or not samples can be assigned  
 377 to the group). Samples in this group include multiple catchments but with a large component from Ilulissat  
 378 (32% of datapoints) and Nuup Kangerlua (55% of datapoints), both of which were over-represented  
 379 compared to their proportional importance in the sub-dataset where they each constituted 18% of  
 380 datapoints. Antarctic samples and samples from Eqip Sermia were under-represented in this ~1:1 group,



381 accounting for 0 and 2 (9%) samples, respectively, despite contributing 26% and 20% of the samples with  
382 all macronutrients detectable. The ~1:1 datapoints all refer to summertime so cannot easily be explained  
383 as mistaken sea ice samples. Furthermore, observed nutrient concentrations were often too high to be  
384 explained by carry-over from seawater contamination (see Section 3.2). The ratios of  $\text{dSi}:\text{NO}_3^-$  also did  
385 not consistently match the ratio in near-surface fjord water samples where this was collected in parallel  
386 with icebergs. Whilst the  $\text{dSi}:\text{NO}_3^-$  ratio in most near-surface samples from the Ilulissat Icefjord in August  
387 2022 was ~1 ( $1.39 \pm 0.61$ ,  $n=25$  in August 2022), for Nuup Kangerlua in August and September 2019 the  
388 ratio of  $\text{dSi}:\text{NO}_3^-$  was always  $>18$  (Krause et al., 2021). A ~1:1  $\text{NO}_x^-:\text{dSi}$  ratio in ice nevertheless  
389 resembles a marine origin.

### 390 **3.2 Evaluating reproducibility and potential sampling biases**

391 Glacial ice can usually be visually distinguished from sea ice due to its distinct texture, colour and  
392 morphology. For meltwater samples that were tested for salinity, values were always  $<0.3$  psu. However,  
393 even minor traces of seawater in samples would be sufficient to impart a measurable macronutrient  
394 concentration change because ice macronutrient concentrations were generally very low compared to  
395 pelagic macronutrient concentrations in the corresponding sampling regions. This is particularly the case  
396 at the Antarctic sample sites where high macronutrient concentrations of 20-80  $\mu\text{M}$   $\text{dSi}$ , 1-2  $\mu\text{M}$   $\text{PO}_4^{3-}$   
397 and 10-30  $\mu\text{M}$   $\text{NO}_3^-$  are relatively typical of marine waters (e.g. Höfer et al., 2019; Forsch et al., 2021;  
398 Trefault et al., 2021). Close to marine-terminating glaciers in the Arctic, macronutrient concentrations in  
399 near-surface waters can still be elevated relative to the low concentrations reported for ice, e.g. 1-30  $\mu\text{M}$   
400  $\text{dSi}$ , 0.2-0.7  $\mu\text{M}$   $\text{PO}_4^{3-}$  and 0-10  $\mu\text{M}$   $\text{NO}_3^-$  for the inner part of Nuup Kangerlua (Krause et al., 2021; Meire  
401 et al., 2017). Thus, seawater macronutrient concentrations were generally equal to, or greater than ice  
402 concentrations at the locations where ice calves.

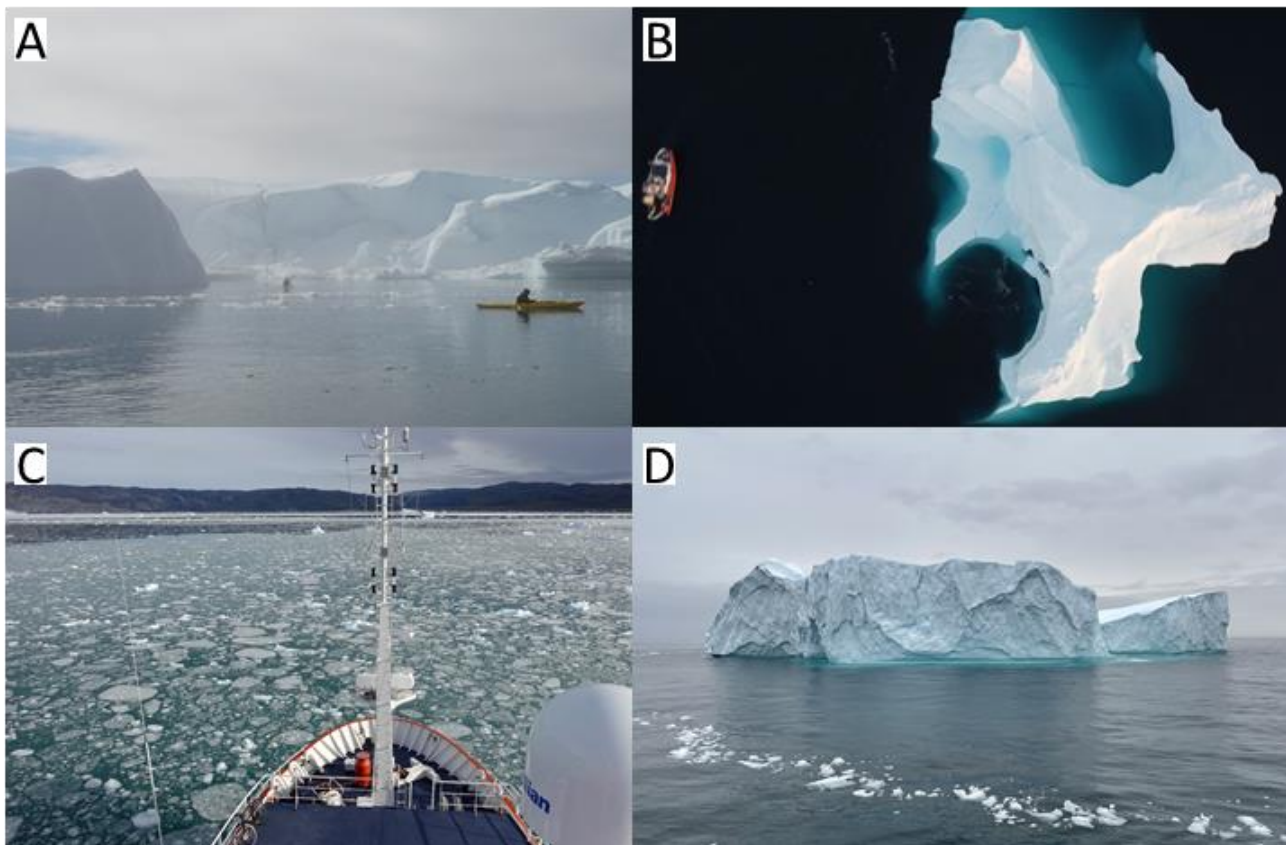
403  
404 Using the maximum observed marine macronutrient concentrations for our Antarctic sampling locations,  
405 assuming no detectable macronutrients in ice and that salinity of 0.3 exclusively reflected the carry-over  
406 of seawater from sampling, nutrient concentrations of up to 0.26  $\mu\text{M}$   $\text{NO}_3^-$ , 0.02  $\text{PO}_4^{3-}$   $\mu\text{M}$  and 0.069  $\mu\text{M}$   
407  $\text{dSi}$  could be observed as a seawater contamination signal. The rinsing procedure used to collect samples

408 herein whereby ice was sequentially melted, with the meltwater then used to swill and rinse the sample  
409 bag, was designed precisely to minimize trace metal contamination and three such rinses undertaken  
410 correctly would theoretically remove ~99.99% of any saline water collected with an ice sample in addition  
411 to any contamination from ice handling. This would also not leave a detectable ( $>0.01$ ) salinity increase  
412 in the collected sample such that any detected salinity would have to come from ice melt. Sea ice samples  
413 were not targeted for sampling herein, but two samples were collected during the 2017 Pia fjord campaign  
414 (Patagonia) alongside calved ice samples and measured macronutrient concentrations were: 2.00 and 5.97  
415  $\mu\text{M NO}_x^-$ , 0.08 and 0.13  $\mu\text{M PO}_4^{3-}$ , 0.28 and 0.63  $\mu\text{M dSi}$ . These sea ice  $\text{NO}_x^-$  and dSi concentrations  
416 were above average compared to freshwater ice samples collected in the same location (Supp. Table 2).  
417 Similarly, samples of land fast sea ice from Antarctica generally have high concentrations of all  
418 macronutrients compared to iceberg samples reported herein (Grotti et al., 2005; Günther and Dieckmann,  
419 1999; Nomura et al., 2023). It is apparent from the ratio of  $\text{NO}_x^-$ :  $\text{PO}_4^{3-}$ :dSi in sea ice that the high nutrient  
420 concentration in sea ice have a saline origin (Henley et al., 2023). Sampling protocols for sea ice are  
421 however different in several aspects particularly the application of a sequential rinsing (for glacial ice,  
422 but not for sea ice) and ambient temperatures during sample collection. A sequential rinsing with sea ice,  
423 as applied herein, might lead to an uneven distribution of nutrients in meltwater samples due to the layered  
424 structure of sea ice and the effects of brine channels (Ackley and Sullivan, 1994; Gleitz et al., 1995;  
425 Vancoppenolle et al., 2010). With the possible exceptions of regions that experience ice mélange (a  
426 mixture of sea ice and icebergs) and/or marine ice, glacial ice is expected to be more homogenous with  
427 respect to salinity. In prior work we also demonstrated no sustained trend in Fe concentrations when  
428 aliquots of meltwater were collected from ice fragments in series (Hopwood et al., 2016). A further critical  
429 difference with sea ice samples concerns ambient conditions as all ice samples collected herein were  
430 obtained from seawater with temperatures  $>0^\circ\text{C}$  i.e. under conditions where ice was melting when it was  
431 collected. Conversely, a large fraction of sea ice cores studied to date refer to conditions without *in situ*  
432 melt occurring (Henley et al., 2023).

433

434 During the dedicated iceberg cruise campaign GLICE in Disko Bay (August 2022), ice collection was  
435 confined to 4 subregions of interest (Fig. 4, Supp. Table 3). There was partial ice cover in Disko Bay

436 during boreal summer, which was mainly limited to a patch of high iceberg density close to the outflow  
437 of Ilulissat Icefjord. Combined with the confined nature of the coastal fjords sampled and the relatively  
438 fast disintegration of smaller ice fragments, it was possible to identify with a high degree of certainty the  
439 origin of ice within each subregion (Fig. 4). Within the fjord system hosting the marine-terminating  
440 glacier Eqip Sermia, ice fragments were highly likely to have originated from either Eqip Sermia itself  
441 or, if not, from adjacent calving fronts in the same fjord. Similarly, close to the outflow of Ilulissat  
442 Icefjord, ice fragments were highly likely to have originated from Sermeq Kujalleq. Ice slicks which were  
443 visibly observed to calve from two offshore icebergs within an hour prior to sample collection each  
444 constituted an additional subregion of interest. The two icebergs, referred to herein as ‘Narwhal’ and  
445 ‘Beluga’ were both isolated from other floating ice features with maximum dimensions above the  
446 waterline of >100 m width and >20 m height (Fig. 4). Radar measurements determined that ‘Narwhal’  
447 was approximately stationary throughout the observation period (~12 hours) likely pirouetting on an area  
448 of shallow bathymetry. Iceberg ‘Beluga’ was free-floating and proceeding northwards along a trajectory  
449 through the area which hosted the highest observed iceberg densities in Disko Bay over the cruise duration  
450 (mid-August 2022).



451

452 Figure 4. Ice sample collection areas in four distinct regions of Disko Bay. A Icebergs grounded on the  
 453 sill at the entrance to the Ilulissat Icefjord. B An offshore iceberg which was grounded during the sampling  
 454 period referred to herein as iceberg ‘Narwhal’. C Ice fragments in front of the marine-terminating glacier  
 455 Eqip Sermia. D An offshore iceberg which was free-floating during the sampling period referred to herein  
 456 as iceberg ‘Beluga’.

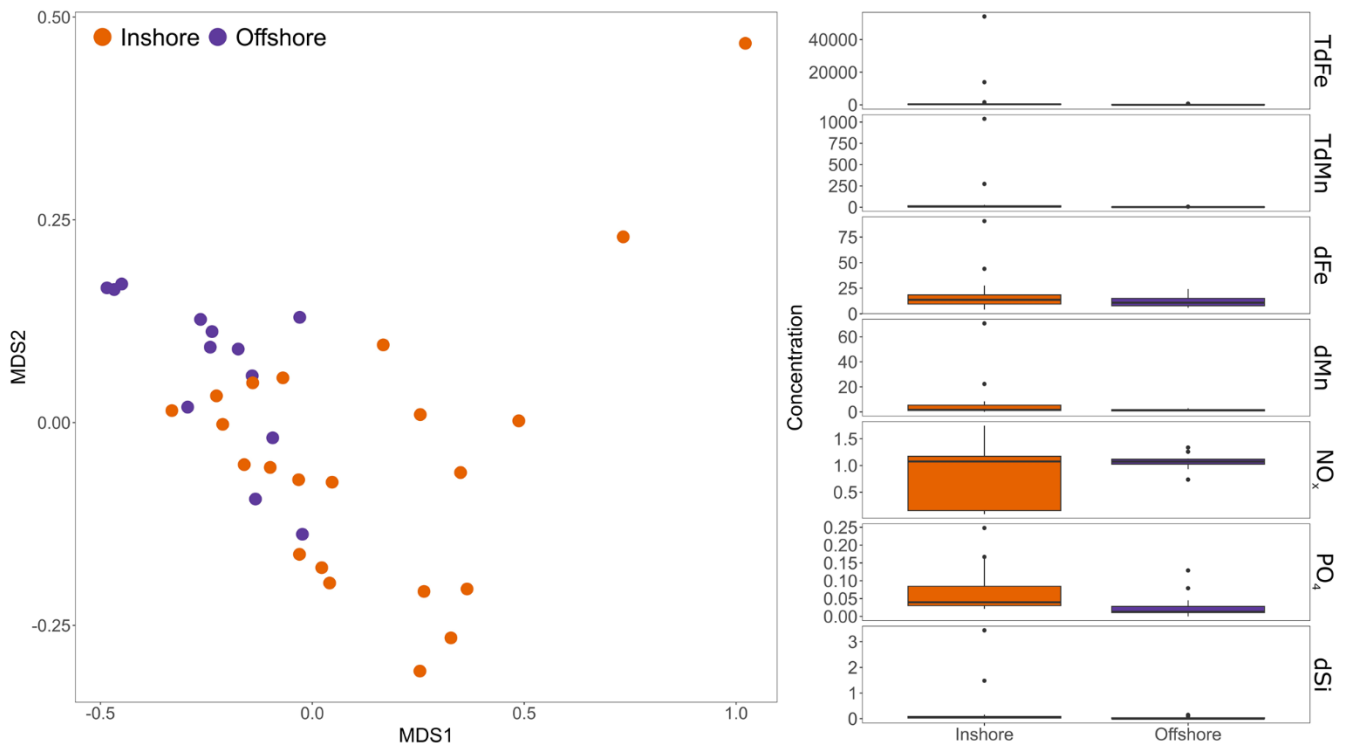
457

458 Ice from the 4 sampled subregions in Disko Bay was similar in all cases with overlapping ranges for the  
 459  $\text{NO}_x^-$ ,  $\text{PO}_4^{3-}$  and dSi concentrations of ice at different locations (Fig. 5). A PERMANOVA analysis  
 460 showed small, but significant, differences ( $R^2 = 0.15$ , p value = 0.002) in the chemical composition of  
 461 iceberg samples collected inshore (Groups A and C, Fig. 4) or offshore (Groups B and D, Fig. 4) in Disko  
 462 Bay when combining groups. An ordination analysis (nMDS stress = 0.04) showed that offshore icebergs  
 463 were grouped together on the left side of the ordination, whereas inshore icebergs were more common on

464 the right side of the ordination (Fig. 5). In general, offshore and inshore icebergs presented similar  
465 concentrations of all nutrients in most of the samples, except for a few inshore samples that had higher  
466 concentrations of all nutrients (Fig. 5). When testing these differences for each individual nutrient, only  
467  $\text{PO}_4^{3-}$  showed significant differences between the two categories (p value = 0.035), with offshore icebergs  
468 showing lower concentrations (Fig. 5). The difference between inshore and offshore ice, whilst present,  
469 was therefore relatively modest.

470

471 Further insight can be gained from a comparison of all data available from Nuup Kangerlua, a relatively  
472 well-studied glacier fjord in southwest Greenland. The fjord hosts three marine-terminating glaciers with  
473 heavy ice mélange cover observed in the inner fjord year-round and some sea ice in the inner fjord during  
474 winter. Samples were collected from the fjord during five independent field campaigns from 2014 to 2019  
475 in different seasons from May in boreal spring to September in boreal autumn. Considering the number  
476 of parameters sampled and the relatively high standard deviation of almost all parameters relative to the  
477 mean or median measured concentrations, there was limited evidence for any seasonal or inter-campaign  
478 differences (Supp. Table 4). No significant differences ( $p > 0.05$ ) were found between groups of samples  
479 obtained at the same field site when organizing the complete dataset by field site and defining each  
480 separate field campaign as a group.



481

482 Figure 5. Comparison of nutrient concentrations from inshore and offshore ice samples collected in Disko  
 483 Bay (August 2022, see Fig. 4). *Left* An ordination analysis (nMDS) comparing concentrations of all  
 484 nutrients measured in ice contrasting inshore and offshore areas of Disko Bay. A PERMANOVA analysis  
 485 of iceberg nutrient concentrations showed weak but significant differences between both areas ( $R^2 = 0.15$ ,  
 486  $p$  value = 0.002). *Right* A direct comparison of all nutrient concentrations for the same dataset. Units:  $\mu\text{M}$   
 487 for dSi,  $\text{NO}_x^-$  and  $\text{PO}_4^{3-}$ ; nM for all trace metals. Only  $\text{PO}_4^{3-}$  showed a significant difference between the  
 488 two categories ( $p$  value = 0.035).

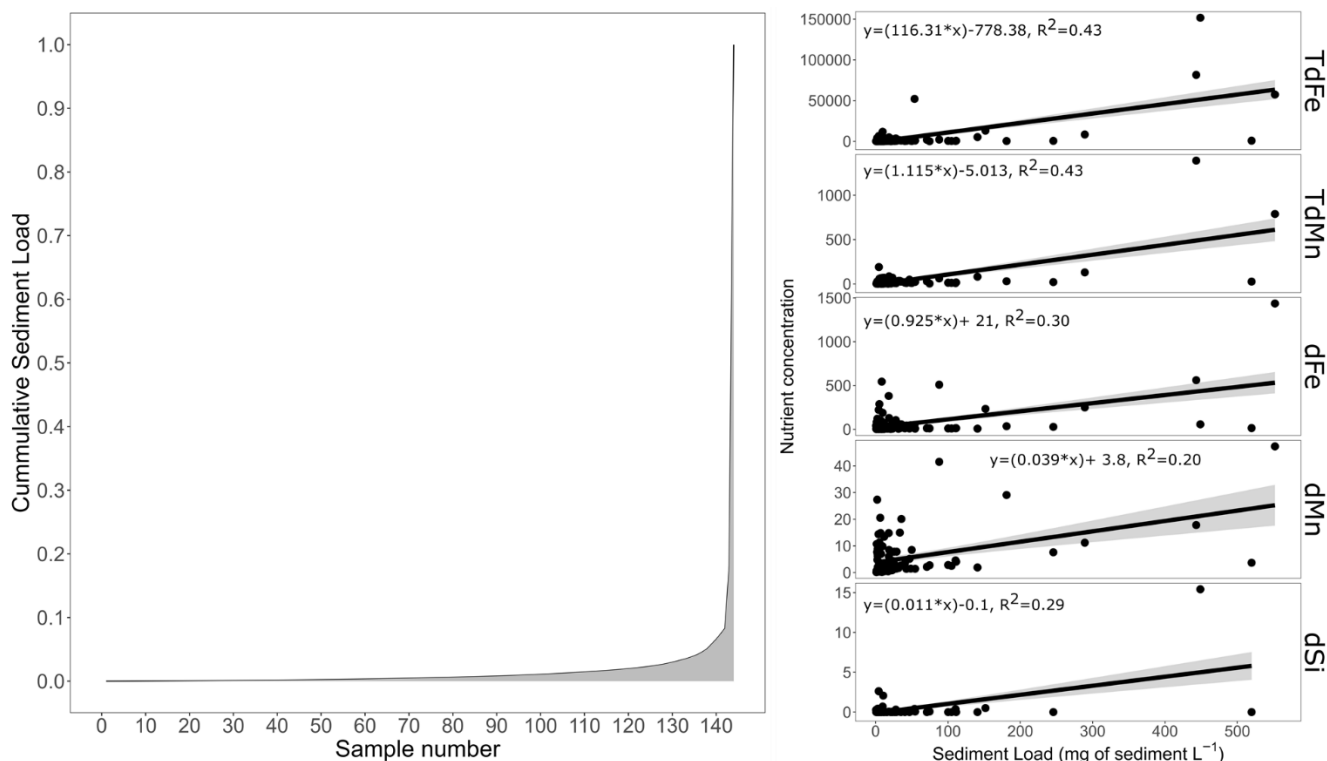
### 489 3.3 Sediment load within icebergs and its relationship with nutrient concentration

490 The sediment load within icebergs collected around the Antarctic Peninsula was highly variable with a  
 491 maximum of  $5072 \text{ mg L}^{-1}$  and a minimum of  $0.69 \text{ mg L}^{-1}$  (median  $8.5 \text{ mg L}^{-1}$  and mean  $430.5 \text{ mg L}^{-1}$ ).  
 492 Particle loads were assessed in three Antarctic locations. The median dry mass was similar across three  
 493 areas, but the mean ( $\pm$  standard deviation) dry mass was more variable due to the occasional sample with  
 494 a high sediment load. Mean dry masses across three areas were: Maxwell Bay, King George Island, (n=65)

495 910 ± 6300 mg L<sup>-1</sup>; Thunder Bay and Neumayer Channel, Wiencke Island, (n=19) 35 ± 110 mg L<sup>-1</sup>; and  
496 South Bay, Doumer Island, (n=60) 39 ± 98 mg L<sup>-1</sup>. Median sediment loads in the three regions were 12,  
497 2.5 and 7.7 mg L<sup>-1</sup>, respectively. The heterogeneous distribution of sediments was reflected in the fact  
498 that ~2% of samples collected contributed ~90% of the total sediment retrieved from the iceberg samples  
499 collectively (Fig. 6). This distribution is similar to previous analysis regarding TdFe (Hopwood et al.,  
500 2019), and sediment load in icebergs from Svalbard (Hopwood et al., 2017). It also qualitatively matches  
501 the distribution of TdMn and TdFe observed herein (see Section 3.1).

502

503 As Fe, Mn and dSi might have sedimentary origins, we tested if there were any significant relationships  
504 between the sediment load of an iceberg and the concentration of each macronutrient and both total  
505 dissolvable and dissolved trace metals (Fig. 6). For NO<sub>x</sub><sup>-</sup> and PO<sub>4</sub><sup>3-</sup> there was no significant relationship  
506 between sediment load and concentration (p values of 0.18 and 0.26 respectively). This is consistent with  
507 the hypothesis that these nutrients primarily have an atmospheric deposition origin which contributes only  
508 a minor fraction of the sediment load to bulk ice. Conversely, TdFe, TdMn, dFe, dMn and dSi all had  
509 significant relationships with sediment load. The concentrations of the total dissolvable fraction of trace  
510 metals showed better fits (TdFe R<sup>2</sup> = 0.43, p value <0.001; TdMn R<sup>2</sup> = 0.43, p value <0.001), than the  
511 dissolved phases of metals (dFe R<sup>2</sup> = 0.30, p value <0.001; dMn R<sup>2</sup> = 0.20, p value <0.001) and dSi (R<sup>2</sup>  
512 = 0.28, p value <0.001). This is consistent with the expectation that englacial sediment drives a direct  
513 enrichment in TdFe and TdMn, which increase proportionately with sediment load. The enrichment of  
514 dFe, dMn and dSi is more variable and may depend on the specific conditions that sediment and ice  
515 experience between englacial sediment incorporation and sample collection.



516

517 Figure 6. Iceberg sediment load and its relationship with nutrient concentrations. *Left* The uneven release  
 518 of sediment in randomly collected ice samples from the Antarctic Peninsula. *Right* The relationship  
 519 between nutrient concentrations and sediment load for ice samples from the Antarctic Peninsula (no  
 520 samples from elsewhere determined sediment load on the same ice fragments as nutrient concentrations).  
 521 Only significant ( $p$  value  $<0.001$ ) relationships are shown. No significant relationship was evident for  
 522 sediment load with nitrate or phosphate. Units:  $\mu\text{M}$  for dSi, nM for all trace metals.

523

524 On several occasions in Nuup Kangerlua and Maxwell Bay we observed structures up to several  
 525 centimetres wide/deep on iceberg surfaces akin to cryoconite holes both above and below the waterline.  
 526 The sediment within such holes was easily disturbed when approaching ice fragments. The regular  
 527 agitation and movement of floating ice fragments and the chaotic nature of calving events suggests that  
 528 cryoconite holes on icebergs formed *in situ* rather than being relics of a glacier surface prior to calving.  
 529 This raises an interesting question about whether sediment-rich layers and any associated nutrients could  
 530 be subject to disintegration mechanisms distinct from bulk ice. When large ice samples weighing 10-45



531 kg were stored in the dark at 5-10°C, higher loads of sediment were released in the initial melt fractions  
532 (Supp. Fig. 1). This trend was highly reproducible occurring in all observed experiments (n=8) when large  
533 ice samples specifically targeted for their high englacial sediment loads were retained. The sediment  
534 release rate declined with an exponential logarithmic function over the first 48 hours (Supp. Figure 1). It  
535 should be noted that randomly collected samples had much lower sediment loads (Fig. 6).

## 536 **4 Discussion**

### 537 **4.1 Insights into nutrient origins from ratios**

538 There are several distinct mechanisms via which ice could accumulate different nutrient ratios.  
539 Precipitation and aerosol on ice surfaces would be expected to deposit  $\text{NO}_x^-$  and  $\text{PO}_4^{3-}$  (Fischer et al.,  
540 1998; Kjær et al., 2015), assuming a limited biogeochemical imprint from surface biological (or  
541 photochemical) processes. Atmospheric deposition of  $\text{NO}_x^-$  and  $\text{PO}_4^{3-}$  varies regionally. Snow  $\text{NO}_3^-$   
542 deposition over central Greenland is reported as  $1.21 \pm 0.19 \mu\text{mol kg}^{-1}$  for recent and  $0.56 \pm 0.19 \mu\text{mol}$   
543  $\text{kg}^{-1}$  for pre-industrial values (Fischer et al., 1998). Reported concentrations of  $\text{PO}_4^{3-}$  are more sensitive  
544 to the method used due to universally low concentrations. Phosphate concentrations in ice from the last  
545 glacial period in Greenland are reported to range from 3 to 62 nM (Kjær et al., 2015). These ranges are  
546 similar to the  $\text{NO}_3^-$  and  $\text{PO}_4^{3-}$  values we report for Greenlandic calved ice herein: mean ( $\pm$  standard  
547 deviation)  $0.78 \pm 0.69 \text{NO}_3^-$ , median  $0.74 \text{NO}_3^-$ , mean  $36 \pm 50 \text{nM PO}_4^{3-}$ , and median  $28 \text{nM PO}_4^{3-}$ . Modern  
548 atmospheric deposition is expected to impact the N:P ratio as atmospheric pollution is generally  
549 associated with higher N:P ratios (e.g. Peñuelas et al., 2012) and could explain the increase in N:P ratio  
550 at higher  $\text{NO}_3^-$  concentrations. Atmospheric deposition of  $\text{NO}_3^-$  in Antarctica is less directly affected by  
551 anthropogenic emissions, but the ranges of  $\text{NO}_3^-$  reported for snow and ice samples overlap with the  
552 corresponding values for Greenland e.g. ranges of 0.08-2.12  $\mu\text{M}$  (Akers et al., 2022) and 0.29-2.58  $\mu\text{M}$   
553 (Neubauer & Heumann., 1988).

554

555 In addition to an atmospheric deposition signal in ice macronutrient concentrations for  $\text{NO}_x^-$  and  $\text{PO}_4^{3-}$ ,  
556 some degree of sedimentary signal might also affect dSi concentrations due to release of dSi from glacier-

557 associated weathering processes (Halbach et al., 2019; Wadham et al., 2010). In contrast no, or very  
558 limited, release of  $\text{NO}_3^-$  or  $\text{PO}_4^{3-}$  is expected from weathering which is supported by the correlations  
559 herein (Fig. 6). Sediment associated with an iceberg could be from basal layers, other englacial sediment  
560 entrained prior to calving, or acquired from scouring events subsequent to calving. Shallow areas of all  
561 field sites herein had grounded icebergs. In Disko Bay during 2 weeks of cruise observations in August  
562 2022 for example, the majority of large (>100 m width above water line) icebergs were observed to be  
563 grounded. In terms of TdFe, TdMn, dFe, dMn and dSi we hypothesize that two categories of sediment  
564 may be distinguishable. Englacial sediment with little biogeochemical processing should retain a  
565 TdFe:TdMn ratio which is close to the crustal abundance ratio of Fe:Mn, with low dFe, dMn and dSi  
566 concentrations. Basal sediment layers, particularly from catchments with warm-based glaciers, may have  
567 a similar TdFe:TdMn ratio but higher concentrations of dFe, dMn and dSi due to more active  
568 biogeochemical processing in subglacial environments (e.g. Wadham et al., 2010; Tranter et al., 2005).  
569 Finally, scoured sediments acquired after calving could constitute a broad range of compositions  
570 considering the gradient in benthic conditions along glacier fjords (Laufer-Meiser et al., 2021; Wehrmann  
571 et al., 2013) and may accordingly contain more biogenic and/or authigenic phases than englacial sediment.  
572 These sediments may be highly variable in composition but should impart high TdFe and TdMn  
573 concentrations, with varying Fe:Mn ratios, and high dFe, dMn and dSi concentrations. Basal sediments  
574 and scoured sediments from fjord environments therefore probably cannot be distinguished  
575 unambiguously from concentrations measured herein alone. Yet we can likely distinguish englacial  
576 sediment from basal or scoured sediment. Dissolved Si concentrations were low across the whole dataset,  
577 suggesting basal ice was a very small component of sampled ice. The linear relationship between TdFe  
578 and TdMn across a wide range of observed concentrations also suggests minimal incorporation of  
579 authigenic mineral phases and, in combination with low dSi, hints that basal ice from warm-based glaciers  
580 is largely absent from this dataset. This is consistent with the expectation that basal layers are lost prior  
581 to, or rapidly following, iceberg calving (Smith et al., 2019). In contrast, in runoff sampled close to iceberg  
582 sampling regions, dSi concentrations were elevated (range 1.2-44  $\mu\text{M}$ ) and often considerably higher than  
583 concentrations measured in ice melt (Supp. Table 2).

584

585 The weak, but significant, relationships with dSi, dFe, dMn and sediment load; and the stronger  
586 relationships between TdFe and TdMn and sediment load are consistent both with a sedimentary origin  
587 of these components and the caveats that further physical and/or biogeochemical processing mechanisms  
588 have to be considered to fully explain the distributions of dSi, dFe and dMn (Fig. 6). As the concentrations  
589 of  $\text{NO}_x^-$  and  $\text{PO}_4^{3-}$  were consistent with an atmospheric origin, a varying concentration of dSi from  
590 sedimentary sources could also easily explain the observed trend in the  $\text{NO}_x^-$ :dSi and  $\text{PO}_4^{3-}$ :dSi ratios.  
591 Whilst elevated dFe and dMn concentrations in runoff reflect release of these phases from glacier-derived  
592 sediments (Hawkings et al., 2020; Raiswell, 2011), the concentrations herein for ice melt were not  
593 strongly correlated with each other or sediment load (Fig. 6). This could reflect the origin of dissolved Fe  
594 and Mn from distinct, different mineral phases, yet dFe concentrations generally correlate poorly with  
595 other trace elements in aquatic environments due to rapid scavenging onto particle surfaces and rapid  
596 aggregation of colloids (which are included within the '<0.2  $\mu\text{m}$ ' definition of dissolved herein) (Zhang  
597 et al., 2015). A poor correlation could also therefore reflect the tendency for inorganic dFe species to  
598 become rapidly scavenged close to source (Lippiatt et al., 2010). Measured concentrations herein refer to  
599 freshly collected meltwater so it is difficult to establish how dFe concentrations may have changed during  
600 the ice melting process. Conversely, dMn species are more stable in solution, especially in the photic zone  
601 (Sunda et al., 1983; Sunda and Huntsman, 1988), and this is often reflected in much higher dMn:dFe  
602 ratios in proglacial aquatic environments than would be expected based on crustal abundances (e.g. van  
603 Genuchten et al., 2022; Hawkings et al., 2020; Yang et al., 2022). Curiously, dSi also correlated poorly  
604 with all metal phases. This again could simply reflect different mineral phases driving elevated dSi, dFe  
605 and dMn concentrations (van Genuchten et al., 2022). Yet considering all of these elements are expected  
606 to be released from labile phases present in glacier-derived sediments, at least within specific regions  
607 some degree of correlation might be expected. Further work to quantify the rates of gross and net dFe,  
608 dMn and dSi release under *in situ* conditions within ice and frozen sediment layers, could perhaps  
609 elucidate processes via which net release of these components may be uncoupled. Photochemical  
610 processes are particularly likely to affect Fe and Mn release (Kim et al., 2010; Kim et al., 2024), and the  
611 scavenging potential of Mn and Fe species (van Genuchten et al., 2022) may also be important in terms

612 of how they interact with other dissolved and particulate components of the ice-sediment-meltwater  
613 matrix.

614

#### 615 **4.2 Key role of sediment-rich layers, and their disintegration, for nutrient release**

616 Several works have speculated that Arctic and Antarctic icebergs may have distinct differences in  
617 sediment load, with the former generally having higher sediment loads than the later (Anderson et al.,  
618 1980). However, there are several observer biases in making such comparisons. Arctic icebergs are  
619 generally smaller due to the prevalence of tidewater glacier-derived ice rather than large ice shelves.  
620 Furthermore, due to the much easier logistical situation for observers in the Arctic, Arctic icebergs are  
621 more easily observed in coastal environments than Antarctic icebergs. Ice observed at a distance often  
622 appears cleaner than is the case upon closer inspection where sediment layers can be better identified.  
623 Nevertheless, a comparison of smaller ice fragments from Kongsfjorden in Svalbard and three localities  
624 in the Antarctic Peninsula showed that the former had higher sediment loads. Mean sediment loads of 21  
625  $\text{g L}^{-1}$  (median  $0.58 \text{ g L}^{-1}$ ) were previously reported for Kongsfjorden (Hopwood et al., 2019). Average  
626 sediment load values for ice fragments handled similarly from the Antarctic Peninsula were  $8.5 \text{ mg L}^{-1}$   
627 (median) and mean  $430.5 \text{ mg L}^{-1}$  (mean), respectively, which are considerably lower. Contrasting  
628 warm/cold-based glaciers and the higher exposed land/ice cover ratio of the coastal glaciated Arctic may  
629 explain much of this difference.

630

631 Sediment-rich layers within icebergs have long been hypothesized to be particularly important for the  
632 delivery of the micronutrient Fe into the ocean (Hart, 1934) and this has been explicitly confirmed with  
633 measurements of dFe and particulate Fe (Lin et al., 2011; Raiswell, 2011). We verify herein, that sediment  
634 distribution is a major factor explaining TdFe and TdMn distribution, yet suggest this is a less important  
635 factor in explaining dFe, dMn and dSi distribution in icebergs (Fig. 5). The dynamics of sediment-rich  
636 layers and their fate in the marine environment is of special interest for trace metal biogeochemistry given  
637 the (co)-limiting role these micronutrients have for phytoplankton growth in the Southern Ocean (Hawco  
638 et al., 2022; Martin et al., 1990b). Yet multiple factors are likely important for determining the delivery  
639 of dFe and dMn to the marine environment because these fluxes do not simply scale with sediment input

640 as per TdFe and TdMn. A close association of TdFe and TdMn is perhaps unsurprising and corroborates  
641 a lithogenic origin for the vast majority of Fe present in icebergs. It also suggests limited biogeochemical  
642 processing of englacial material and/or rapid loss of basal ice layers preventing the modification of a  
643 lithogenic ratio in-between sediment acquisition by icebergs and sediment release in the ocean (Forsch et  
644 al., 2021).

645

646 A curious observation herein was that cryoconite formation was observed on ice fragments suggesting  
647 that, as is the case on glacier surfaces (Cook et al., 2015; Rozwalak et al., 2022), this can be an important  
648 process affecting sediment dynamics on icebergs. The unstable nature of icebergs, especially smaller  
649 icebergs, means that cryoconite holes are likely to be shorter lived than their glacier counterparts, but they  
650 still may constitute an important feature via which iceberg embedded sediment is processed. The  
651 accumulation of sediment as cryoconite could for example impede photochemical processing of particles,  
652 but also potentially create micro-gradients in O<sub>2</sub>, pH and temperature that result in different chemical  
653 conditions than if particles were homogenously distributed (Rozwalak et al., 2022). On larger, more stable  
654 tabular icebergs, cryoconite may facilitate the growth of attached diatoms (Ferrario et al., 2012; Robison  
655 et al., 2011). These processes are well described on glacier surfaces but a critical difference in interpreting  
656 their significance in iceberg environments is that iceberg movement and rolling is likely to prevent the  
657 long-term development of cryoconite on anything other than large tabular icebergs. Nevertheless, the  
658 observation of such holes at centimetre size in environments where icebergs are free floating and rapidly  
659 disintegrating suggests that they might constitute an underappreciated mechanism of iceberg melt and  
660 sediment processing.

661

662 A further, to our knowledge, novel observation was the tendency of embedded sediment to be rapidly  
663 discharged from ice fragments. When collecting larger pieces of ice it was found that, in all cases,  
664 embedded sediment was rapidly washed out of the ice fragments largely within the melting of the first  
665 10-20% of ice volume (Supp. Fig. 1). These ice fragments were specifically targeted to avoid ice with  
666 surface sediment layers and so this result cannot be explained by the loss of sediment frozen on the surface  
667 of ice. If this process was occurring at larger scales in nature it could further act to skew the deposition of

668 iceberg-borne particles towards inshore environments i.e. it would compound the inefficiencies in the  
669 delivery of sediment and associated nutrients to the offshore marine environment due to the rapid loss of  
670 basal ice layers. The mechanism of this process is unclear but it is not associated with ongoing cryoconite  
671 formation or similar associated processes due to albedo effects because the ice was stored in the dark.

### 672 673 **4.3 (Micro)nutrient fluxes to the ocean from icebergs**

674  
675 By combining measured concentrations herein with estimates of the ice volume discharged from  
676 Greenland and Antarctica, annual flux estimates can be estimated for (micro)nutrients associated with  
677 icebergs (Table 1). For the macronutrients  $\text{NO}_3^-$ ,  $\text{PO}_4^{3-}$ , and dSi, the uncertainty in these flux estimates  
678 remains large relative to the magnitude of the flux. This is an inherent result of the large fraction of ice  
679 with macronutrient concentrations close to the LOD, so would not be changed with further data collection.  
680 Iceberg-derived macronutrient fluxes are likely minor in terms of annual polar pelagic nutrient cycling  
681 (Table 1) and in most coastal environments will dilute, rather than enhance, ambient macronutrient  
682 concentrations. This is especially the case in Antarctic waters, where macronutrient concentrations are  
683 universally high (Boyer et al., 2018). The low macronutrient of ice also implies that physical effects  
684 associated with iceberg passage, mixing and any stratification resulting from meltwater are likely larger  
685 effects on annual macronutrient budgets for biota than the direct contribution of meltwater (Helly et al.,  
686 2011; Tarling et al., 2024). In regions where meltwater from icebergs accumulates in a thin surface layer,  
687 which is a phenomenon largely confined to Arctic fjords (e.g. Enderlin et al., 2016), low macronutrient  
688 concentrations may contribute to low primary production in near-surface layers. Although it should be  
689 noted that meltwater delivery is not confined to the surface (Moon et al., 2018) and, as noted, can drive  
690 the vertical entrainment of macronutrients within the water column.

691  
692  
693  
694

<b>Nutrient</b>	<b>Greenland Ice Sheet annual discharge Mmol yr<sup>-1</sup></b>	<b>Antarctic Ice Sheet annual discharge Mmol yr<sup>-1</sup></b>
NO <sub>3</sub> <sup>-</sup>	389 ± 345 (370)	418 ± 796 (168)
PO <sub>4</sub> <sup>3-</sup>	18 ± 25 (14)	76 ± 83 (58)
dSi	212 ± 701 (27)	476 ± 2187 (b/d)
dFe	7.1 ± 15 (3.9)	130 ± 472 (18)
dMn	2.3 ± 6.0 (0.77)	32 ± 191 (3.3)

695 Table 1. Annual fluxes of nutrients associated with icebergs assuming calved ice volumes of 500 km<sup>3</sup> yr<sup>-1</sup>  
696 <sup>1</sup> from Greenland and 1100 km<sup>3</sup> yr<sup>-1</sup> from Antarctica (Bamber et al., 2018; Rignot et al., 2013). Values  
697 are mean ± standard deviation (median); ‘b/d’ represents a median sample below detection.

698

699 Delivery of total dissolvable Fe and Mn fluxes from icebergs to the ocean may be considerable (Table 1),  
700 but, as these components are associated with heterogeneous particle-rich layers in ice, their delivery may  
701 be skewed towards inshore waters where primary production is less limited by trace metal availability.  
702 Dissolved Fe and Mn components are of more direct relevance to phytoplankton demands on the short-  
703 term timescales associated with iceberg passage, due to the short residence time of particle associated  
704 metal phases in the marine environment. Annual dFe and dMn fluxes also carry relatively large  
705 uncertainties (Table 1) which reflects the wide range of concentrations present in ice. Although the crustal  
706 abundance of Mn oxides is approximately 50× lower than that of Fe oxides (Rudnick and Gao, 2004),  
707 dMn fluxes from Greenland and Antarctica are 32% and 25% of the corresponding dFe fluxes,  
708 respectively (Table 1). Similar trends are evident in dFe and dMn concentrations within fjord  
709 environments where trace metals from subglacial discharge and runoff enter the ocean (Forsch et al.,  
710 2021; van Genuchten et al., 2022). The relatively-high concentrations of dMn compared to dFe likely  
711 reflect the rapid scavenging of dFe close to source compared to more conservative behaviour of dMn over  
712 short (hours to days) timescales (Kandel and Aguilar-Islas, 2021; Yang et al., 2022; Zhang et al., 2015).

713

714 A key finding throughout was that the macronutrient and micronutrient content of ice was relatively  
715 similar between catchments and regions worldwide despite the contrasting geographic context of Arctic

716 and Antarctic ice calving fronts and notable differences in sediment loads between regions (Fig. 2). There  
717 was limited evidence of differences in ice nutrient concentrations between field campaigns returning to  
718 the same location (Nuup Kangerlua, southwest Greenland) in different seasons/years and similarly limited  
719 evidence of differences contrasting ice fragments collected offshore in Disko Bay (west Greenland), with  
720 ice fragments collected inshore close to marine-terminating glacier fronts (Fig. 5). Icebergs are inherently  
721 heterogenous due to the nature of englacial and basal sediment incorporation and loss processes. This  
722 heterogeneity combined with generally low nutrient concentrations, appears to mask and regional or  
723 catchment specific trends in macronutrient or micronutrient content related to changing bedrock  
724 composition (e.g. Halbach et al., 2019), calving dynamics (Smith et al., 2019), or photochemical processes  
725 (e.g. Kim et al., 2010).

726  
727 Whilst further sampling would not reduce uncertainty in the estimated nutrient fluxes (Table 1), some  
728 specific caveats with our present work could be resolved in the future. Herein we have considered only  
729  $\text{NO}_x^-$  as a source of bioaccessible nitrogen, but considering the universally low concentrations present in  
730 icebergs, other N sources (e.g. DON- Dissolved Organic Nitrogen, and  $\text{NH}_4$ ) may be relatively important.  
731 We hypothesized that a basal ice influence would be present in some ice fragments with high dSi  
732 alongside dFe and dMn, but conversely found very low dSi concentrations across all field locations.  
733 Future process studies might elucidate the mechanistic reasons why elevated dSi concentrations are not  
734 present alongside dFe and dMn concentrations in ice melt. Finally, sediment rich layers of large ice  
735 samples were observed to rapidly melt, potentially indicating that these layers are prone to disintegration.  
736 Such a mechanism could be an important regulator of sediment dispersion in the marine environment,  
737 potentially further skewing the delivery of iceberg rafted debris and nutrients towards coastal waters.

## 738 739 **5 Conclusions**

740 The dataset reported here covers ice fragments collected from a range of Arctic and Antarctic, polar and  
741 (sub)polar marine-terminating glaciers, and floating ice tongues. Throughout, icebergs are found to be  
742 only a minor source of macronutrients to the ocean with a large fraction of measurements close to, or



743 below the standard analytical detection limit. Icebergs do however deliver modest fluxes of dissolved Fe  
744 and Mn to the polar oceans, which are likely important ecologically- particularly in the Southern Ocean  
745 (Sedwick et al., 2000; Wu et al., 2019). The rapid dilution of meltwater close to icebergs, typically to  
746 concentrations <1% (Helly et al., 2011; Stephenson et al., 2011), means these trace metal inputs are  
747 challenging to constrain from in-situ pelagic observations (Lin et al., 2011), thus our measurements  
748 provide a first order constraint on iceberg-derived micronutrient fluxes into polar seas. The scavenged-  
749 type behaviour of dFe may explain why the dFe:dMn ratio in ice melt is considerably higher than expected  
750 from crustal abundances of Fe and Mn oxides, yet this also raises questions about how micronutrients  
751 sourced from icebergs behave immediately after release into the ocean. Dissolved Fe may be scavenged  
752 close to source limiting the spatial extent of Fe-fertilization from iceberg tracks, whereas, especially in  
753 the photic zone, dMn is more stable in seawater (Sunda et al., 1983). Thus icebergs may be an even more  
754 disproportionately important dMn source to biota than the dFe:dMn ratio in meltwater suggests.

755

## 756 **6 Data availability**

757 New data presented herein is available from SeaDataNet [  
758 [https://emodnet.ec.europa.eu/geonetwork/emodnet/api/records/ff3c625c-6a39-46ef-b329-  
759 222040f85917](https://emodnet.ec.europa.eu/geonetwork/emodnet/api/records/ff3c625c-6a39-46ef-b329-222040f85917), last accessed 20/08/2024]. Literature data was compiled from prior published values (De  
760 Baar et al., 1995; Campbell and Yeats, 1982; Forsch et al., 2021; Höfer et al., 2019; Hopwood et al., 2017,  
761 2019; Lin et al., 2011; Loscher et al., 1997; Martin et al., 1990b). For convenience, a merged dataset is  
762 appended for data not previously compiled.

## 763 **7 Author contribution**

764 MH, DC, JH and EPA designed the study and acquired funding and resources. JK, DC, JD, JH, EA, TL,  
765 LM and MH conducted field work. EA, KZ and MH conducted laboratory analysis. JK, JH and MH  
766 conducted data analysis. JK and MH wrote the initial draft of the paper and all authors contributed to  
767 revision of the text.

## 768 **8 Competing interests**

769 The authors declare that they have no conflict of interest.

## 770 **9 Acknowledgements**

771 Tim Steffens (GEOMAR) is thanked for technical assistance with ICP-MS, André Mutzberg (GEOMAR)  
772 for macronutrient data, Stephan Krisch (formerly GEOMAR), Thomas Juul-Pedersen (GINR) and Case  
773 van Genuchten (GEUS) for assistance with sampling. The captain and crew of RV Sanna are thanked for  
774 field support. Antarctic sampling was possible through FONDAP-IDEAL 15150003 and FONDECYT-  
775 Regular 1211338 (awarded to JH). MH received support from the DFG (HO 6321/1-1), the GLACE  
776 project organised by the Swiss Polar Institute and supported by the Swiss Polar Foundation, NSFC project  
777 42150610482 and the European Union H2020 research and innovation programme under grant agreement  
778 n° 824077. LM was funded by research programme VENI with project number 016.Veni.192.150  
779 financed by the Dutch Research Council (NWO). JD was sponsored by a scholarship from the Instituto  
780 Antártico Chileno (INACH), Correos de Chile, and the Fuerza Aérea de Chile (FACH). Ship time and  
781 work in Nuup Kangerlua was conducted in collaboration with MarineBasis-Nuuk, part of the Greenland  
782 Ecosystem Monitoring project (GEM). We gratefully acknowledge logistics and funding contributions  
783 from the Danish Centre for Marine Research (DCH), Greenland Institute of Natural Resources, Novo  
784 Nordic Foundation (NNF17SH0028142) and INACH.

## 785 **10 References**

786 Ackley, S. F. and Sullivan, C. W.: Physical controls on the development and characteristics of Antarctic sea ice biological  
787 communities— a review and synthesis, *Deep Sea Research Part I: Oceanographic Research Papers*, 41, 1583–1604,  
788 [https://doi.org/10.1016/0967-0637\(94\)90062-0](https://doi.org/10.1016/0967-0637(94)90062-0), 1994.

789  
790 Akers, P. D., Savarino, J., Caillon, N., Servettaz, A. P. M., Le Meur, E., Magand, O., Martins, J., Agosta, C., Crockford, P.,  
791 Kobayashi, K., Hattori, S., Curran, M., van Ommen, T., Jong, L., & Roberts, J. L. (2022). Sunlight-driven nitrate loss records  
792 Antarctic surface mass balance. *Nature Communications*, 13(1), 4274. <https://doi.org/10.1038/s41467-022-31855-7>

793

794 Alley, R. B., Cuffey, K. M., Evenson, E. B., Strasser, J. C., Lawson, D. E., and Larson, G. J.: How glaciers entrain and transport  
795 basal sediment: Physical constraints, *Quat Sci Rev*, 16, 1017–1038, [https://doi.org/10.1016/S0277-3791\(97\)00034-6](https://doi.org/10.1016/S0277-3791(97)00034-6), 1997.  
796

797 Anderson, J. B., Domack, E. W., and Kurtz, D. D.: Observations of Sediment-laden Icebergs in Antarctic Waters: Implications  
798 to Glacial Erosion and Transport, *Journal of Glaciology*, 25, 387–396, <https://doi.org/10.3189/S0022143000015240>, 1980.  
799

800 De Baar, H. J. W., De Jong, J. T. M., Bakker, D. C. E., Loscher, B. M., Veth, C., Bathmann, U., and Smetacek, V.: Importance  
801 of iron for plankton blooms and carbon dioxide drawdown in the Southern Ocean, *Nature*, 373, 412–415,  
802 <https://doi.org/10.1038/373412a0>, 1995.  
803

804 Bamber, J. L., Tedstone, A. J., King, M. D., Howat, I. M., Enderlin, E. M., van den Broeke, M. R., and Noel, B.: Land Ice  
805 Freshwater Budget of the Arctic and North Atlantic Oceans: 1. Data, Methods, and Results, *J Geophys Res Oceans*, 123, 1827–  
806 1837, <https://doi.org/10.1002/2017JC013605>, 2018.  
807

808 Boyd, P. W., Arrigo, K. R., Strzepek, R., and Van Dijken, G. L.: Mapping phytoplankton iron utilization: Insights into Southern  
809 Ocean supply mechanisms, *J Geophys Res Oceans*, 117, <https://doi.org/10.1029/2011JC007726>, 2012.  
810

811 Boyer, T. P., Garcia, H. E., Locarnini, R. A., Zweng, M. M., Mishonov, A. V., Reagan, J. R., Weathers, K. A., Baranova, O.  
812 K., Seidov, D., and Smolyar, I. V.: *World Ocean Atlas 2018*, 2018.  
813

814 Browning, T. J., Achterberg, E. P., Engel, A., and Mawji, E.: Manganese co-limitation of phytoplankton growth and major  
815 nutrient drawdown in the Southern Ocean, *Nat Commun*, 12, 884, <https://doi.org/10.1038/s41467-021-21122-6>, 2021.  
816

817 Campbell, J. A. and Yeats, P. A.: The distribution of manganese, iron, nickel, copper and cadmium in the waters of Baffin Bay  
818 and the Canadian Arctic Archipelago, *Oceanologica Acta*, 5, <https://doi.org/10.1007/s00128-002-0077-7>, 1982.  
819

820 Cantoni, C., Hopwood, M. J., Clarke, J. S., Chiggiato, J., Achterberg, E. P., and Cozzi, S.: Glacial drivers of marine  
821 biogeochemistry indicate a future shift to more corrosive conditions in an Arctic fjord, *J Geophys Res Biogeosci*, 125,  
822 e2020JG005633, <https://doi.org/10.1029/2020JG005633>, 2020.  
823

824 Cook, J., Edwards, A., Takeuchi, N., and Irvine-Fynn, T.: Cryoconite: The dark biological secret of the cryosphere, *Progress*  
825 *in Physical Geography: Earth and Environment*, 40, 66–111, <https://doi.org/10.1177/0309133315616574>, 2015.  
826

827 Craven, M., Allison, I., Fricker, H. A., and Warner, R.: Properties of a marine ice layer under the Amery Ice Shelf, East  
828 Antarctica, *Journal of Glaciology*, 55, 717–728, <https://doi.org/10.3189/002214309789470941>, 2009.

829

830 Dowdeswell, J. A. and Dowdeswell, E. K.: Debris in Icebergs and Rates of Glaci-Marine Sedimentation: Observations from  
831 Spitsbergen and a Simple Model, *J Geol*, 97, 221–231, <https://doi.org/10.1086/629296>, 1989.

832

833 Enderlin, E. M., Hamilton, G. S., Straneo, F., and Sutherland, D. A.: Iceberg meltwater fluxes dominate the freshwater budget  
834 in Greenland’s iceberg-congested glacial fjords, *Geophys Res Lett*, 43, <https://doi.org/10.1002/2016GL070718>, 2016.

835

836 Ferrario, M. E., Cefarelli, A. O., Robison, B., and Vernet, M.: *Thalassioneis signyensis* (bacillariophyceae) from northwest  
837 Weddell Sea icebergs, an emendation of the generic description, *J Phycol*, 48, 222–230, <https://doi.org/10.1111/j.1529-8817.2011.01097.x>, 2012.

838

839

840 Fischer, H., Wagenbach, D., and Kipfstuhl, J.: Sulfate and nitrate firm concentrations on the Greenland ice sheet: 1. Large-  
841 scale geographical deposition changes, *Journal of Geophysical Research: Atmospheres*, 103, 21927–21934,  
842 <https://doi.org/10.1029/98JD01885>, 1998.

843

844 Fischer, H., Schüpbach, S., Gfeller, G., Bigler, M., Röthlisberger, R., Erhardt, T., Stocker, T. F., Mulvaney, R., and Wolff, E.  
845 W.: Millennial changes in North American wildfire and soil activity over the last glacial cycle, *Nat Geosci*, 8, 723–727,  
846 <https://doi.org/10.1038/ngeo2495>, 2015.

847

848 Forsch, K. O., Hahn-Woernle, L., Sherrell, R. M., Roccanova, V. J., Bu, K., Burdige, D., Vernet, M., and Barbeau, K. A.:  
849 Seasonal dispersal of fjord meltwaters as an important source of iron and manganese to coastal Antarctic phytoplankton,  
850 *Biogeosciences*, 18, 6349–6375, <https://doi.org/10.5194/bg-18-6349-2021>, 2021.

851

852 van Genuchten, C. M., Hopwood, M. J., Liu, T., Krause, J., Achterberg, E. P., Rosing, M. T., and Meire, L.: Solid-phase Mn  
853 speciation in suspended particles along meltwater-influenced fjords of West Greenland, *Geochim Cosmochim Acta*, 326, 180–  
854 198, <https://doi.org/10.1016/j.gca.2022.04.003>, 2022.

855

856 Gleitz, M., v.d. Loeff, M. R., Thomas, D. N., Dieckmann, G. S., and Millero, F. J.: Comparison of summer and winter inorganic  
857 carbon, oxygen and nutrient concentrations in Antarctic sea ice brine, *Mar Chem*, 51, 81–91, [https://doi.org/10.1016/0304-4203\(95\)00053-T](https://doi.org/10.1016/0304-4203(95)00053-T), 1995.

858

859

860 Grotti, M., Soggia, F., Ianni, C., and Frache, R.: Trace metals distributions in coastal sea ice of Terra Nova Bay, Ross Sea,  
861 Antarctica, *Antarct Sci*, 17, 289–300, <https://doi.org/10.1017/S0954102005002695>, 2005.

862

863 Günther, S. and Dieckmann, G. S.: Seasonal development of algal biomass in snow-covered fast ice and the underlying platelet  
864 layer in the Weddell Sea, Antarctica, *Antarct Sci*, 11, 305–315, <https://doi.org/10.1017/S0954102099000395>, 1999.

865

866 Gutt, J., Starmans, A., and Dieckmann, G.: Impact of iceberg scouring on polar benthic habitats, *Mar Ecol Prog Ser*, 137, 311–  
867 316, <https://doi.org/10.3354/meps137311>, 1996.

868

869 Halbach, L., Vihtakari, M., Duarte, P., Everett, A., Granskog, M. A., Hop, H., Kauko, H. M., Kristiansen, S., Myhre, P. I.,  
870 Pavlov, A. K., Pramanik, A., Tatarek, A., Torsvik, T., Wiktor, J. M., Wold, A., Wulff, A., Steen, H., and Assmy, P.: Tidewater  
871 Glaciers and Bedrock Characteristics Control the Phytoplankton Growth Environment in a Fjord in the Arctic,  
872 <https://doi.org/10.3389/fmars.2019.00254>, 2019.

873

874 Hansen, H. P. and Koroleff, F.: Determination of nutrients, in: *Methods of seawater analysis*, edited by: Grasshoff, K., K.  
875 Kremling, and Ehrhardt, M., Wiley-VCH Verlag GmbH, 159–228, 1999.

876

877 Hansson, M. E.: The Renland ice core. A Northern Hemisphere record of aerosol composition over 120,000 years, *Tellus B:*  
878 *Chemical and Physical Meteorology*, 46, 390–418, 1994.

879

880 Hart, T. J.: *Discovery Reports*, *Discovery Reports*, VIII, 1–268, 1934.

881

882 Hawco, N. J., Tagliabue, A., and Twining, B. S.: Manganese Limitation of Phytoplankton Physiology and Productivity in the  
883 Southern Ocean, *Global Biogeochem Cycles*, 36, e2022GB007382, <https://doi.org/10.1029/2022GB007382>, 2022.

884

885 Hawkings, J. R., Wadham, J. L., Benning, L. G., Hendry, K. R., Tranter, M., Tedstone, A., Nienow, P., and Raiswell, R.: Ice  
886 sheets as a missing source of silica to the polar oceans, 8, 14198, 2017.

887

888 Hawkings, J. R., Skidmore, M. L., Wadham, J. L., Priscu, J. C., Morton, P. L., Hatton, J. E., Gardner, C. B., Kohler, T. J.,  
889 Stibal, M., Bagshaw, E. A., Steigmeyer, A., Barker, J., Dore, J. E., Lyons, W. B., Tranter, M., and Spencer, R. G. M.: Enhanced  
890 trace element mobilization by Earth’s ice sheets, *Proceedings of the National Academy of Sciences*, 117, 31648–31659,  
891 <https://doi.org/10.1073/pnas.2014378117>, 2020.

892

893 Helly, J. J., Kaufmann, R. S., Stephenson Jr., G. R., and Vernet, M.: Cooling, dilution and mixing of ocean water by free-  
894 drifting icebergs in the Weddell Sea, *Deep-Sea Research Part II-Topical Studies in Oceanography*, 58, 1346–1363,  
895 <https://doi.org/10.1016/j.dsr2.2010.11.010>, 2011.

896

897 Henley, S. F., Cozzi, S., Fripiat, F., Lannuzel, D., Nomura, D., Thomas, D. N., Meiners, K. M., Vancoppenolle, M., Arrigo,  
898 K., Stefels, J., van Leeuwe, M., Moreau, S., Jones, E. M., Fransson, A., Chierici, M., and Delille, B.: Macronutrient  
899 biogeochemistry in Antarctic land-fast sea ice: Insights from a circumpolar data compilation, *Mar Chem*, 104324,  
900 <https://doi.org/10.1016/j.marchem.2023.104324>, 2023.

901

902 Herraiz-Borreguero, L., Lannuzel, D., van der Merwe, P., Treverrow, A., and Pedro, J. B.: Large flux of iron from the Amery  
903 Ice Shelf marine ice to Prydz Bay, East Antarctica, *J Geophys Res Oceans*, 121, 6009–6020,  
904 <https://doi.org/10.1002/2016JC011687>, 2016.

905

906 Höfer, J., González, H., Laudien, J., Schmidt, G., Häussermann, V., and Richter, C.: All you can eat: the functional response  
907 of the cold-water coral *Desmophyllum dianthus* feeding on krill and copepods, *PeerJ*, 6, <https://doi.org/10.7717/peerj.5872>,  
908 2018.

909

910 Höfer, J., Giesecke, R., Hopwood, M. J. M. J., Carrera, V., Alarcón, E., and González, H. E. H. E.: The role of water column  
911 stability and wind mixing in the production/export dynamics of two bays in the Western Antarctic Peninsula, *Prog Oceanogr*,  
912 174, 105–116, <https://doi.org/10.1016/j.pocean.2019.01.005>, 2019.

913

914 Hopwood, M. J., Connelly, D. P., Arendt, K. E., Juul-Pedersen, T., Stinchcombe, M. C., Meire, L., Esposito, M., and Krishna,  
915 R.: Seasonal changes in Fe along a glaciated Greenlandic fjord, *Front Earth Sci (Lausanne)*, 4,  
916 <https://doi.org/10.3389/feart.2016.00015>, 2016.

917

918 Hopwood, M. J., Cantoni, C., Clarke, J. S., Cozzi, S., and Achterberg, E. P.: The heterogeneous nature of Fe delivery from  
919 melting icebergs, *Geochem Perspect Lett*, 3, 200–209, <https://doi.org/10.7185/geochemlet.1723>, 2017.

920

921 Hopwood, M. J., Carroll, D., Höfer, J., Achterberg, E. P., Meire, L., Le Moigne, F. A. C., Bach, L. T., Eich, C., Sutherland,  
922 D. A., and González, H. E.: Highly variable iron content modulates iceberg-ocean fertilisation and potential carbon export,  
923 *Nat Commun*, 10, 5261, <https://doi.org/10.1038/s41467-019-13231-0>, 2019.

924

925 Huhn, O., Rhein, M., Kanzow, T., Schaffer, J., and Sültenfuß, J.: Submarine Meltwater From Nioghalvfjærdsbræ (79 North  
926 Glacier), Northeast Greenland, *J Geophys Res Oceans*, 126, e2021JC017224, <https://doi.org/10.1029/2021JC017224>, 2021.

927

928 Kandel, A. and Aguilar-Islas, A.: Spatial and temporal variability of dissolved aluminum and manganese in surface waters of  
929 the northern Gulf of Alaska, *Deep Sea Research Part II: Topical Studies in Oceanography*, 104952,  
930 <https://doi.org/10.1016/j.dsr2.2021.104952>, 2021.

931

932 Kim, J., Park, Y. K., Koo, T., Jung, J., Kang, I., Kim, K., Park, H., Yoo, K.-C., Rosenheim, B. E., & Conway, T. M. (2024).  
933 Microbially-mediated reductive dissolution of Fe-bearing minerals during freeze-thaw cycles. *Geochimica et Cosmochimica*  
934 *Acta*, 376, 134–143. <https://doi.org/10.1016/j.gca.2024.05.015>

935

936 Kim, K., Choi, W., Hoffmann, M. R., Yoon, H.-I., and Park, B.-K.: Photoreductive Dissolution of Iron Oxides Trapped in Ice  
937 and Its Environmental Implications, *Environ Sci Technol*, 44, 4142–4148, <https://doi.org/10.1021/es9037808>, 2010.

938

939 Kjær, H. A., Dallmayr, R., Gabrieli, J., Goto-Azuma, K., Hirabayashi, M., Svensson, A., and Vallelonga, P.: Greenland ice  
940 cores constrain glacial atmospheric fluxes of phosphorus, *Journal of Geophysical Research: Atmospheres*, 120, 10, 810, 822,  
941 <https://doi.org/10.1002/2015JD023559>, 2015.

942

943 Knight, P. G.: The basal ice layer of glaciers and ice sheets, *Quat Sci Rev*, 16, 975–993, [https://doi.org/10.1016/S0277-](https://doi.org/10.1016/S0277-3791(97)00033-4)  
944 [3791\(97\)00033-4](https://doi.org/10.1016/S0277-3791(97)00033-4), 1997.

945

946 Krause, J., Hopwood, M. J., Höfer, J., Krisch, S., Achterberg, E. P., Alarcón, E., Carroll, D., González, H. E., Juul-Pedersen,  
947 T., Liu, T., Lodeiro, P., Meire, L., and Rosing, M. T.: Trace Element (Fe, Co, Ni and Cu) Dynamics Across the Salinity  
948 Gradient in Arctic and Antarctic Glacier Fjords, *Front Earth Sci (Lausanne)*, 9, 878, <https://doi.org/10.3389/feart.2021.725279>,  
949 2021.

950

951 Krause, J. W., Duarte, C. M., Marquez, I. A., Assmy, P., Fernández-Méndez, M., Wiedmann, I., Wassmann, P., Kristiansen,  
952 S., and Agustí, S.: Biogenic silica production and diatom dynamics in the Svalbard region during spring, *Biogeosciences*, 15,  
953 6503–6517, <https://doi.org/10.5194/bg-15-6503-2018>, 2018.

954

955 Krause, J. W., Schulz, I. K., Rowe, K. A., Dobbins, W., Winding, M. H. S., Sejr, M. K., Duarte, C. M., and Agustí, S.: Silicic  
956 acid limitation drives bloom termination and potential carbon sequestration in an Arctic bloom, *Sci Rep*,  
957 <https://doi.org/10.1038/s41598-019-44587-4>, 2019.

958

959 Krisch, S., Browning, T. J., Graeve, M., Ludwichowski, K.-U., Lodeiro, P., Hopwood, M. J., Roig, S., Yong, J.-C., Kanzow,  
960 T., and Achterberg, E. P.: The influence of Arctic Fe and Atlantic fixed N on summertime primary production in Fram Strait,  
961 North Greenland Sea, *Sci Rep*, 10, 15230, <https://doi.org/10.1038/s41598-020-72100-9>, 2020.

962

963 Latour, P., Wuttig, K., van der Merwe, P., Strzepek, R. F., Gault-Ringold, M., Townsend, A. T., Holmes, T. M., Corkill, M.,  
964 and Bowie, A. R.: Manganese biogeochemistry in the Southern Ocean, from Tasmania to Antarctica, *Limnol Oceanogr*, 66,  
965 2547–2562, <https://doi.org/10.1002/lno.11772>, 2021.

966

967 Laufer-Meiser, K., Michaud, A. B., Maisch, M., Byrne, J. M., Kappler, A., Patterson, M. O., Røy, H., and Jørgensen, B. B.:  
968 Potentially bioavailable iron produced through benthic cycling in glaciated Arctic fjords of Svalbard, *Nat Commun*, 12, 1349,  
969 <https://doi.org/10.1038/s41467-021-21558-w>, 2021.

970

971 Lewis, E. L. and Perkin, R. G.: Ice pumps and their rates, *J Geophys Res Oceans*, 91, 11756–11762,  
972 <https://doi.org/10.1029/JC091iC10p11756>, 1986.

973

974 Lin, H. and Twining, B. S.: Chemical speciation of iron in Antarctic waters surrounding free-drifting icebergs, *Mar Chem*,  
975 128, 81–91, <https://doi.org/10.1016/j.marchem.2011.10.005>, 2012.

976

977 Lin, H., Rauschenberg, S., Hexel, C. R., Shaw, T. J., and Twining, B. S.: Free-drifting icebergs as sources of iron to the  
978 Weddell Sea, *Deep-Sea Research Part II-Topical Studies in Oceanography*, 58, 1392–1406,  
979 <https://doi.org/10.1016/j.dsr2.2010.11.020>, 2011.

980

981 Lippiatt, S. M., Lohan, M. C., and Bruland, K. W.: The distribution of reactive iron in northern Gulf of Alaska coastal waters,  
982 *Mar Chem*, 121, 187–199, <https://doi.org/10.1016/j.marchem.2010.04.007>, 2010.

983

984 Loscher, B. M., DeBaar, H. J. W., DeJong, J. T. M., Veth, C., and Dehairs, F.: The distribution of Fe in the Antarctic  
985 Circumpolar Current, *Deep-Sea Research Part II-Topical Studies in Oceanography*, 44, 143–187,  
986 [https://doi.org/10.1016/S0967-0645\(96\)00101-4](https://doi.org/10.1016/S0967-0645(96)00101-4), 1997.

987

988 Martin, J. H.: Glacial-interglacial CO<sub>2</sub> change : The iron hypothesis, *Paleoceanography*, 5, 1–13, 1990.

989

990 Martin, J. H., Fitzwater, S. E., and Gordon, R. M.: Iron deficiency limits phytoplankton growth in Antarctic waters, *Global*  
991 *Biogeochem Cycles*, 4, 5–12, 1990a.

992



993 Martin, J. H., Gordon, R. M., and Fitzwater, S. E.: Iron in Antarctic waters, *Nature*, 345, 156–158,  
994 <https://doi.org/10.1038/345156a0>, 1990b.

995

996 Meire, L., Meire, P., Struyf, E., Krawczyk, D. W., Arendt, K. E., Yde, J. C., Juul Pedersen, T., Hopwood, M. J., Rysgaard, S.,  
997 and Meysman, F. J. R.: High export of dissolved silica from the Greenland Ice Sheet, *Geophys Res Lett*, 43,  
998 <https://doi.org/10.1002/2016GL070191>, 2016.

999

1000 Meire, L., Mortensen, J., Meire, P., Juul-Pedersen, T., Sejr, M. K., Rysgaard, S., Nygaard, R., Huybrechts, P., and Meysman,  
1001 F. J. R.: Marine-terminating glaciers sustain high productivity in Greenland fjords, *Glob Chang Biol*, 23, 5344–5357,  
1002 <https://doi.org/10.1111/gcb.13801>, 2017.

1003

1004 Moon, T., Sutherland, D. A., Carroll, D., Felikson, D., Kehrl, L., & Straneo, F. (2018). Subsurface iceberg melt key to  
1005 Greenland fjord freshwater budget. *Nature Geoscience*. <https://doi.org/10.1038/s41561-017-0018-z>

1006

1007 Moore, C. M., Mills, M. M., Arrigo, K. R., Berman-Frank, I., Bopp, L., Boyd, P. W., Galbraith, E. D., Geider, R. J., Guieu,  
1008 C., Jaccard, S. L., Jickells, T. D., La Roche, J., Lenton, T. M., Mahowald, N. M., Maranon, E., Marinov, I., Moore, J. K.,  
1009 Nakatsuka, T., Oeschies, A., Saito, M. A., Thingstad, T. F., Tsuda, A., and Ulloa, O.: Processes and patterns of oceanic nutrient  
1010 limitation, *Nature Geosci*, 6, 701–710, <https://doi.org/10.1038/ngeo1765>, 2013.

1011

1012 Mugford, R. I., & Dowdeswell, J. A. (2010). Modeling iceberg-rafted sedimentation in high-latitude fjord environments.  
1013 *Journal of Geophysical Research: Earth Surface*, 115(3). <https://doi.org/10.1029/2009JF001564>

1014

1015 Nielsdottir, M. C., Moore, C. M., Sanders, R., Hinz, D. J., and Achterberg, E. P.: Iron limitation of the postbloom  
1016 phytoplankton communities in the Iceland Basin, *Global Biogeochem Cycles*, 23, <https://doi.org/10.1029/2008gb003410>,  
1017 2009.

1018

1019 Neubauer, J., & Heumann, K. G. (1988). Nitrate trace determinations in snow and firn core samples of ice shelves at the  
1020 weddell sea, Antarctica. *Atmospheric Environment (1967)*, 22(3), 537–545. [https://doi.org/10.1016/0004-6981\(88\)90197-7](https://doi.org/10.1016/0004-6981(88)90197-7)

1021

1022 Nomura, D., Sahashi, R., Takahashi, K. D., Makabe, R., Ito, M., Tozawa, M., Wongpan, P., Matsuda, R., Sano, M., Yamamoto-  
1023 Kawai, M., Nojiri, N., Tachibana, A., Kurosawa, N., Moteki, M., Tamura, T., Aoki, S., and Murase, H.: Biogeochemical  
1024 characteristics of brash sea ice and icebergs during summer and autumn in the Indian sector of the Southern Ocean, *Prog*  
1025 *Oceanogr*, 214, 103023, <https://doi.org/10.1016/j.pocean.2023.103023>, 2023.

1026

1027 Oerter, H., Kipfstuhl, J., Determann, J., Miller, H., Wagenbach, D., Minikin, A., and Graft, W.: Evidence for basal marine ice  
1028 in the Filchner–Ronne ice shelf, *Nature*, 358, 399–401, <https://doi.org/10.1038/358399a0>, 1992.

1029

1030 Oksanen, J., Blanchet, F. G., Friendly, M., Kindt, R., Legendre, P., McGlinn, D., Minchin, P. R., O’Hara, R. B., Simpson, G.  
1031 L., Solymos, P., H., M. H., Stevens, Szoecs, E., and Wagner, H.: *vegan: Community Ecology Package*, 2020.

1032

1033 Parker, B. C., Heiskell, L. E., Thompson, W., and Zeller, E. J.: Non-biogenic fixed nitrogen in Antarctica and some ecological  
1034 implications, *Nature*, 271, 651–652, <https://doi.org/10.1038/271651a0>, 1978.

1035

1036 Peñuelas, J., Sardans, J., Rivas-ubach, A., and Janssens, I. A.: The human-induced imbalance between C, N and P in Earth’s  
1037 life system, *Glob Chang Biol*, 18, 3–6, <https://doi.org/10.1111/j.1365-2486.2011.02568.x>, 2012.

1038

1039 Person, R., Vancoppenolle, M., Aumont, O., and Malsang, M.: Continental and Sea Ice Iron Sources Fertilize the Southern  
1040 Ocean in Synergy, *Geophys Res Lett*, n/a, e2021GL094761, <https://doi.org/10.1029/2021GL094761>, 2021.

1041

1042 R Core Team: *R: A Language and Environment for Statistical Computing*, 2023.

1043

1044 Raiswell, R.: Iceberg-hosted nanoparticulate Fe in the Southern Ocean: Mineralogy, origin, dissolution kinetics and source of  
1045 bioavailable Fe, *Deep-Sea Research Part II-Topical Studies in Oceanography*, 58, 1364–1375,  
1046 <https://doi.org/10.1016/j.dsr2.2010.11.011>, 2011.

1047

1048 Raiswell, R., Benning, L. G., Tranter, M., and Tulaczyk, S.: Bioavailable iron in the Southern Ocean: the significance of the  
1049 iceberg conveyor belt, *Geochem Trans*, 9, <https://doi.org/10.1186/1467-4866-9-7>, 2008.

1050

1051 Raiswell, R., Hawkings, J. R., Benning, L. G., Baker, A. R., Death, R., Albani, S., Mahowald, N., Krom, M. D., Poulton, S.  
1052 W., Wadham, J., and Tranter, M.: Potentially bioavailable iron delivery by iceberg-hosted sediments and atmospheric dust to  
1053 the polar oceans, *Biogeosciences*, 13, 3887–3900, <https://doi.org/10.5194/bg-13-3887-2016>, 2016.

1054

1055 Randelhoff, A., Holding, J., Janout, M., Sejr, M. K., Babin, M., Tremblay, J. É., and Alkire, M. B.: Pan-Arctic Ocean Primary  
1056 Production Constrained by Turbulent Nitrate Fluxes, *Front Mar Sci*, <https://doi.org/10.3389/fmars.2020.00150>, 2020.

1057

1058 Redfield, A. C.: On the proportions of organic derivations in sea water and their relation to the composition of plankton, in:  
1059 *James Johnstone Memorial Volume*, edited by: Daniel, R. J., University Press of Liverpool, Liverpool, 177–192, 1934.

1060

1061 Rignot, E., Jacobs, S., Mouginot, J., and Scheuchl, B.: Ice-Shelf Melting Around Antarctica, *Science* (1979), 341, 266–270,  
1062 <https://doi.org/10.1126/science.1235798>, 2013.

1063

1064 Robison, B. H., Vernet, M., and Smith, K. L.: Algal communities attached to free-drifting, Antarctic icebergs, *Deep Sea*  
1065 *Research Part II: Topical Studies in Oceanography*, 58, 1451–1456, <https://doi.org/10.1016/j.dsr2.2010.11.024>, 2011.

1066

1067 Rozwalak, P., Podkowa, P., Buda, J., Niedzielski, P., Kawecki, S., Ambrosini, R., Azzoni, R. S., Baccolo, G., Ceballos, J. L.,  
1068 Cook, J., Di Mauro, B., Ficetola, G. F., Franzetti, A., Ignatiuk, D., Klimaszyk, P., Łokas, E., Ono, M., Parnikoza, I., Pietryka,  
1069 M., Pittino, F., Poniecka, E., Porazinska, D. L., Richter, D., Schmidt, S. K., Sommers, P., Souza-Kasprzyk, J., Stibal, M.,  
1070 Szczuciński, W., Uetake, J., Wejnerowski, Ł., Yde, J. C., Takeuchi, N., and Zawierucha, K.: Cryoconite – From minerals and  
1071 organic matter to bioengineered sediments on glacier’s surfaces, *Science of The Total Environment*, 807, 150874,  
1072 <https://doi.org/10.1016/j.scitotenv.2021.150874>, 2022.

1073

1074 Rudnick, R. L. and Gao, S.: Composition of the continental crust, in: *Treatise on geochemistry*, vol 3 *The Crust*, edited by:  
1075 Holland, H. D. and Turekian, K. K., Elsevier, Amsterdam, 1–65, 2004.

1076

1077 Ryan-Keogh, T. J., Macey, A. I., Nielsdottir, M. C., Lucas, M. I., Steigenberger, S. S., Stinchcombe, M. C., Achterberg, E. P.,  
1078 Bibby, T. S., and Moore, C. M.: Spatial and temporal development of phytoplankton iron stress in relation to bloom dynamics  
1079 in the high-latitude North Atlantic Ocean, *Limnol Oceanogr*, 58, 533–545, <https://doi.org/10.4319/lo.2013.58.2.0533>, 2013.

1080

1081 Schwarz, J. N. and Schodlok, M. P.: Impact of drifting icebergs on surface phytoplankton biomass in the Southern Ocean:  
1082 Ocean colour remote sensing and in situ iceberg tracking, *Deep Sea Res 1 Oceanogr Res Pap*, 56, 1727–1741,  
1083 <https://doi.org/10.1016/j.dsr.2009.05.003>, 2009.

1084

1085 Sedwick, P. N., DiTullio, G. R., and Mackey, D. J.: Iron and manganese in the Ross Sea, Antarctica: Seasonal iron limitation  
1086 in Antarctic shelf waters, *Journal of Geophysical Research-Oceans*, 105, 11321–11336, <https://doi.org/10.1029/2000jc000256>,  
1087 2000.

1088

1089 Shaw, T. J., Raiswell, R., Hexel, C. R., Vu, H. P., Moore, W. S., Dudgeon, R., and Smith Jr., K. L.: Input, composition, and  
1090 potential impact of terrigenous material from free-drifting icebergs in the Weddell Sea, *Deep-Sea Research Part II-Topical*  
1091 *Studies in Oceanography*, 58, 1376–1383, <https://doi.org/10.1016/j.dsr2.2010.11.012>, 2011.

1092

1093 Shulenberger, E. (1983). Water-column studies near a melting Arctic iceberg. *Polar Biology*, 2(3), 149–158.  
1094 <https://doi.org/10.1007/BF00448964>

1095  
1096 Smith Jr., K. L., Robison, B. H., Helly, J. J., Kaufmann, R. S., Ruhl, H. A., Shaw, T. J., Twining, B. S., and Vernet, M.: Free-  
1097 drifting icebergs: Hot spots of chemical and biological enrichment in the Weddell Sea, *Science* (1979), 317, 478–482,  
1098 <https://doi.org/10.1126/science.1142834>, 2007.  
1099  
1100 Smith, J. A., Graham, A. G. C., Post, A. L., Hillenbrand, C.-D., Bart, P. J., and Powell, R. D.: The marine geological imprint  
1101 of Antarctic ice shelves, *Nat Commun*, 10, 5635, <https://doi.org/10.1038/s41467-019-13496-5>, 2019.  
1102  
1103 Stephenson, G. R., Sprintall, J., Gille, S. T., Vernet, M., Helly, J. J., and Kaufmann, R. S.: Subsurface melting of a free-floating  
1104 Antarctic iceberg, *Deep Sea Research Part II: Topical Studies in Oceanography*, 58, 1336–1345,  
1105 <https://doi.org/10.1016/j.dsr2.2010.11.009>, 2011.  
1106  
1107 Stibal, M., Box, J. E., Cameron, K. A., Langen, P. L., Yallop, M. L., Mottram, R. H., Khan, A. L., Molotch, N. P., Christmas,  
1108 N. A. M., Cali Quaglia, F., Remias, D., Smeets, C. J. P. P., van den Broeke, M. R., Ryan, J. C., Hubbard, A., Tranter, M., van  
1109 As, D., and Ahlstrøm, A. P.: Algae Drive Enhanced Darkening of Bare Ice on the Greenland Ice Sheet, *Geophys Res Lett*, 44,  
1110 11, 411–463, 471, <https://doi.org/10.1002/2017GL075958>, 2017.  
1111  
1112 Sunda, W. G. and Huntsman, S. A.: Effect of sunlight on redox cycles of manganese in the southwestern Sargasso Sea, *Deep*  
1113 *Sea Research Part A, Oceanographic Research Papers*, 35, 1297–1317, [https://doi.org/10.1016/0198-0149\(88\)90084-2](https://doi.org/10.1016/0198-0149(88)90084-2), 1988.  
1114  
1115 Sunda, W. G., Huntsman, S. a., and Harvey, G. R.: Photoreduction of manganese oxides in seawater and its geochemical and  
1116 biological implications, *Nature*, 301, 234–236, <https://doi.org/10.1038/301234a0>, 1983.  
1117  
1118 Syvitski, J. P. M., Burrell, D. C., & Skei, J. M. (1987). *Fjords*. Springer New York. [https://doi.org/10.1007/978-1-4612-4632-](https://doi.org/10.1007/978-1-4612-4632-9)  
1119 9  
1120  
1121 Tarling, G. A., Thorpe, S. E., Henley, S. F., Burson, A., Liszka, C. M., Manno, C., Lucas, N. S., Ward, F., Hendry, K. R.,  
1122 Malcolm S. Woodward, E., Wootton, M., and Povl Abrahamsen, E.: Collapse of a giant iceberg in a dynamic Southern Ocean  
1123 marine ecosystem: In situ observations of A-68A at South Georgia, *Prog Oceanogr*, 226, 103297,  
1124 <https://doi.org/10.1016/j.pocean.2024.103297>, 2024.  
1125  
1126 Taylor, R. L., Semeniuk, D. M., Payne, C. D., Zhou, J., Tremblay, J.-É., Cullen, J. T., and Maldonado, M. T.: Colimitation by  
1127 light, nitrate, and iron in the Beaufort Sea in late summer, *J Geophys Res Oceans*, 118, 3260–3277,  
1128 <https://doi.org/10.1002/jgrc.20244>, 2013.

1129

1130 Tournadre, J., Bouhier, N., Girard-Arduin, F., and Rémy, F.: Antarctic icebergs distributions 1992–2014, *J Geophys Res*  
1131 *Oceans*, 121, 327–349, <https://doi.org/10.1002/2015JC011178>, 2016.

1132

1133 Tranter, M., Skidmore, M., and Wadham, J.: Hydrological controls on microbial communities in subglacial environments,  
1134 *Hydrol Process*, 19, 995–998, <https://doi.org/10.1002/hyp.5854>, 2005.

1135

1136 Trefault, N., De la Iglesia, R., Moreno-Pino, M., Lopes dos Santos, A., Gériques Ribeiro, C., Parada-Pozo, G., Cristi, A., Marie,  
1137 D., and Vaultot, D.: Annual phytoplankton dynamics in coastal waters from Fildes Bay, Western Antarctic Peninsula, *Sci Rep*,  
1138 11, 1368, <https://doi.org/10.1038/s41598-020-80568-8>, 2021.

1139

1140 Vancoppenolle, M., Goosse, H., de Montety, A., Fichefet, T., Tremblay, B., and Tison, J.-L.: Modeling brine and nutrient  
1141 dynamics in Antarctic sea ice: The case of dissolved silica, *J Geophys Res Oceans*, 115,  
1142 <https://doi.org/10.1029/2009JC005369>, 2010.

1143

1144 Vernet, M., Sines, K., Chakos, D., Cefarelli, A. O., and Ekern, L.: Impacts on phytoplankton dynamics by free-drifting icebergs  
1145 in the NW Weddell Sea, *Deep Sea Research Part II: Topical Studies in Oceanography*, 58, 1422–1435,  
1146 <https://doi.org/10.1016/j.dsr2.2010.11.022>, 2011.

1147

1148 Wadham, J. L., Tranter, M., Skidmore, M., Hodson, A. J., Priscu, J., Lyons, W. B., Sharp, M., Wynn, P., and Jackson, M.:  
1149 Biogeochemical weathering under ice: Size matters, *Global Biogeochem Cycles*, 24, <https://doi.org/10.1029/2009gb003688>,  
1150 2010.

1151

1152 Wadley, M. R., Jickells, T. D., and Heywood, K. J.: The role of iron sources and transport for Southern Ocean productivity,  
1153 *Deep-Sea Research Part I-Oceanographic Research Papers*, 87, 82–94, <https://doi.org/10.1016/j.dsr.2014.02.003>, 2014.

1154

1155 Wehrmann, L. M., Formolo, M. J., Owens, J. D., Raiswell, R., Ferdelman, T. G., Riedinger, N., and Lyons, T. W.: Iron and  
1156 manganese speciation and cycling in glacially influenced high-latitude fjord sediments (West Spitsbergen, Svalbard): Evidence  
1157 for a benthic recycling-transport mechanism, <https://doi.org/10.1016/j.gca.2014.06.007>, 2013.

1158

1159 Woodworth-Lynas, C. M. T., Josenhans, H. W., Barrie, J. V, Lewis, C. F. M., and Parrott, D. R.: The physical processes of  
1160 seabed disturbance during iceberg grounding and scouring, *Cont Shelf Res*, 11, 939–961, [https://doi.org/10.1016/0278-](https://doi.org/10.1016/0278-4343(91)90086-L)  
1161 [4343\(91\)90086-L](https://doi.org/10.1016/0278-4343(91)90086-L), 1991.

1162

1163 Wu, M., McCain, J. S. P., Rowland, E., Middag, R., Sandgren, M., Allen, A. E., and Bertrand, E. M.: Manganese and iron  
1164 deficiency in Southern Ocean *Phaeocystis antarctica* populations revealed through taxon-specific protein indicators, *Nat*  
1165 *Commun*, 10, 3582, <https://doi.org/10.1038/s41467-019-11426-z>, 2019.  
1166  
1167 Wu, S.-Y. and Hou, S.: Impact of icebergs on net primary productivity in the Southern Ocean, *Cryosphere*, 11, 707–722,  
1168 <https://doi.org/10.5194/tc-11-707-2017>, 2017.  
1169  
1170 Yang, Y., Ren, J., and Zhu, Z.: Distributions and Influencing Factors of Dissolved Manganese in Kongsfjorden and Ny-  
1171 Ålesund, Svalbard, *ACS Earth Space Chem*, 6, 1259–1268, <https://doi.org/10.1021/acsearthspacechem.1c00388>, 2022.  
1172  
1173 Zhang, R., John, S. G., Zhang, J., Ren, J., Wu, Y., Zhu, Z., Liu, S., Zhu, X., Marsay, C. M., and Wenger, F.: Transport and  
1174 reaction of iron and iron stable isotopes in glacial meltwaters on Svalbard near Kongsfjorden: From rivers to estuary to ocean,  
1175 *Earth Planet Sci Lett*, 424, 201–211, <https://doi.org/10.1016/j.epsl.2015.05.031>, 2015.  
1176